Mineralogy and Petrology (2000) 69: 109–142

Mineralogy and Petrology

P-T paths and tectonic evolution of shear zones separating high-grade terrains from cratons: examples from Kola Peninsula (Russia) and Limpopo Region (South Africa)

L. L. Perchuk[1,2], **T. V. Gerya**[2,1], **D. D. Van Reenen**[3], **C. A. Smit**[3], and **A. V. Krotov**[1]

[1] Department of Petrology, Geological Faculty, Moscow State University, Moscow, Russia
[2] Institute of Experimental Mineralogy, Russian Academy of Sciences, Chernogolovka, Moscow district, Russia
[3] Department of Geology, Rand Afrikaans University, Johannesburg, Republic of South Africa

With 9 Figures

Received January 29, 1999;
revised version accepted August 10, 1999

Summary

The petrology and *P-T* evolution of mica schists from two regional scale tectonic (shear) zones that separate high grade terrains (''mobile belts'') from cratons are described. These are the 2.4–1.9 Ga Tanaelv Belt, a suture zone that separates the Lapland granulite complex from the Karelian craton (Kola Peninsula–Fennoscandia), and the 2.69 Ga Hout River Shear Zone that separates the > 2.9 Ga Kaapvaal craton from the 2.69 Ga South Marginal Zone of the Limpopo high-grade terrain (South Africa).

Two *metamorphic* zones are identified in strongly deformed mica schists from the 1.9 Ga Korva Tundra Group of the Tanaelv belt: (1) a chlorite-staurolite zone tectonically overlaying gneisses of the Karelian craton, and (2) a kyanite-biotite zone tectonically underlying garnet amphibolites of the Tanaelv Belt, which are in tectonic contact with the Lapland granulite complex. The prograde reaction $Chl + St + Ms \Rightarrow Ky + Bt + Qtz + H_2O$ clearly defines a boundary between zones (1) and (2). Rotated garnet porphyroblasts from zone (1) contain numerous inclusions (*Otz*, *Chl*, *Ms*), and show clear Mg/Fe chemical zoning, suggesting garnet growth during prograde metamorphism. The metamorphic peak, $T = 650\,^{\circ}C$ and $P = 7.5$ kbar, is recorded in the kyanite-biotite zone and characterized by unzoned snowball garnet. In many samples of mica schists euhedral garnet porphyroblasts of the retrograde stage are completely

devoid of mineral inclusions while N_{Mg} decreases from core to rim, indicating a decrease in *P-T* from 650 °C, 7.5 kbar to 530 °C, 5 kbar.

The Hout River Shear Zone (South Africa) shows metamorphic zonation from greenschists through epidote amphibolites to garnet amphibolites. Rare strongly deformed mica schists ($Chl + Grt + Pl + Ms + Bt + Qtz$) occur as thin layers among epidote-amphibolites only. Garnet porphyroblasts in the schists are similar to that of the Tanaelv Belt recording a prograde *P-T* path with peak conditions of $T = 600$ °C and $P \sim 5.5$ kbar. The retrograde stage is documented by the continuous reaction $Prp + 2Ms + Phl \Rightarrow 6Qtz + 3East$ recording a minimum $T = 520$ °C and $P \sim 3.3$ kbar. Similar narrow clockwise *P-T* loops recorded in mica schists from both studied shear zones suggest similarities in the geodynamic history of both shear zones under consideration.

Zusammenfassung

P-T Pfade und tektonische Entwicklung von Scherzonen, die hochgradige Terranes von Kratonen trennen: Zwei Beispiele von der Halbinsel Kola (Russland) und der Limpopo-Region (Südafrika)

Die Petrologie und *P-T* Entwicklung von Glimmerschiefern aus zwei regionalen tektonischen Scherzonen, die hochgradige Terranes (''mobile belts'') von Kratonen trennen, werden beschrieben. Diese sind der 2.4−1.9 Ga Tanaev Belt, eine Suturzone, die die Lappland Granulite vom karelischen Pluton (Halbinsel Kola - Fennoskandien) trennt, sowie die 2.69 Ga Hout River Shear Zone, die den > 2.9 Ga Kaapvaal Kraton von der 2.69 Ga South Marginal Zone des hochgradigen Limpopo Terranes (Südafrika) trennt.

Zwei metamorphe Zonen sind in stark deformierten Glimmerschiefern der 1.9 Ga Korva Tundra Group zu unterscheiden: (1) eine Chlorit-Staurolith-Zone, die den Gneisen des karelischen Kratons auflagert, und (2) eine Kyanit-Biotit-Zone, die die Granatamphibolite des Tanaev Belt unterlagert und in tektonischem Kontakt mit dem Lappland Granulitkomplex steht. Die prograde Reaktion $Chl + St + Ms \Rightarrow Ky + Bt + Qtz + H_2O$ trennt die beiden Zonen. Rotierte Granatporphyroblasten aus der Zone (1) enthalten zahlreiche Einschlüsse (*Qtz*, *Chl*, *Ms*) und zeigen eine Mg/Fe Zonierung, die Granatwachstum während des prograden Metamorphosestadiums nahelegen. Der Metamorphosehöhepunkt (650 °C, 7.5 kbar) wurde in der Kyanit-Biotit-Zone erreicht und ist durch nicht zonierte Schneeballgranate charakterisiert. In vielen Glimmerschieferproben sind die euhedralen Granatporphyroblasten des retrograden Stadiums vollkommen einschlußfrei und N_{Mg} nimmt vom Kern zum Rand hin ab. Das zeigt eine Abnahme der *P-T* Bedingungen von 650 °C, 7.5 kbar auf 530 °C, 5 kbar an. Die Hout River Shear Zone in Südafrika zeigt eine metamorphe Zonierung von Grünschiefern, über Epidotamphibolite zu Granatamphiboliten. Selten kommen stark deformierte Glimmerschiefer ($Chl + Grt + Pl + Ms + Bt + Qtz$) als dünne Lagen zwischen den Epidotamphiboliten vor. Die Granatporphyroblasten sind ähnlich wie die aus dem Tanaev Belt und belegen eine prograde *P-T* Entwicklung mit Peak-Bedingungen von 600 °C und ≈ 5.5 kbar. Das retrograde Stadium ist durch die kontinuierliche Reaktion $Prp + 2Ms + Phl \Rightarrow 6Qtz + 3East$ mit minimal 530 °C und ≈ 3.3 kbar dokumentiert. Die sehr ähnlichen *P-T* Pfade der Glimmerschiefer belegen Ähnlichkeiten in der geodynamischen Geschichte der beiden bearbeiteten Scherzonen.

Introduction

The boundaries between Precambrian granulite facies terrains and adjacent cratons are important keys in understanding the formation and evolution of such

contrasting crustal pairs. Evidence for the thermo- and geodynamic evolution of such boundary areas are often well preserved in terms of structure, mineral equilibria, and chemical zoning of coexisting mineral assemblages. Normally such boundaries are sutures composed of strongly sheared rocks of different initial greenstone lithologies. In addition to the paper by *Perchuk* et al. (1999), this review provides new data that allow to test geodynamic models for the formation of mobile high-grade terrains (e.g., *Perchuk*, 1989, 1991; *Perchuk* et al., 1985, 1992; *Thompson*, 1990; *Roering* et al., 1992a; *Treloar* et al., 1992; *Rollinson* and *Blenkinsop*, 1995; *McCourt* and *Vearncombe*, 1992; *Holzer* et al., 1998).

Apart from new data presented in this paper, related published data and particularly data on regional geology, geochronology and geophysics were taken into account (e.g., *Mikkola*, 1937, 1941; *Eskola*, 1952; *Latyshev*, 1967, 1971; *Merilainen*, 1976; *Priyatkina* and *Sharkov*, 1979; *Barbey* et al., 1980, 1984; *Hörmann* et al., 1980; *Barton* et al., 1983; *Bernard-Griffits* et al., 1984; *Bersthelsen* and *Marker*, 1986; *Krill*, 1985; *van Schalkwyk* et al., 1987; *Marker*, 1988, 1990, 1991; *Gaal* et al., 1989; *Kozlov* et al., 1990; *Miyano* et al., 1990; *Volodichev*, 1990; *van Reenen* et al., 1990, 1992; *Tuisku* and *Laajoki*, 1991; *de Beer* and *Stettler*, 1992; *de Wit* et al., 1992a,b; *McCourt* and *van Reenen*, 1992; *Roering* et al., 1992b; *Smit* et al., 1992; *Tsunogae* et al., 1992; *van Schalkwyk* and *van Reenen*, 1992; *Mitrofanov* et al., 1993; *Perchuk* and *Gerya*, 1995; *Przhjialgovskiy* and *Terekhov*, 1995; *Glebovitskii* et al., 1996; *Mints* et al., 1996; *Perchuk* et al., 1996; *van Reenen* and *Smit*, 1996; *Glebovitskii* and *Efimov*, 1997; *de Wit* and *Ashwal*, 1997; *Kreissig* and *Holzer*, 1997; *Pozhilenko* et al., 1997; *Perchuk* and *Krotov*, 1998; *Perchuk* et al., 1999).

Geology and geochronology

The Tanaelv Belt

The Lapland high grade terrain (HGT*) is situated between the Karelian Craton (KC) in the south and the Inari Craton (IC) in the north (Fig. 1). The Tanaelv Belt (TB) (*Barbey* et al., 1984; *Krill*, 1985), it has been named the Tana Tectonic Belt (e.g., *Kozlov* et al., 1990) in Russia, separates the Lapland complex from the Belomorian complex which represents the northern part of the Karelian craton. A schematic geological map of this area is shown in Fig. 1.

In a number of geological and petrological studies (e.g., *Latyshev*, 1967, 1971; *Priyatkina* and *Sharkov*, 1979; *Krill*, 1985; *Marker*, 1988; *Barbey* and *Raith*, 1990) the TB is regarded as a strongly deformed sequence underlying the Lapland granulite complex and tectonically overlying less deformed rocks of the Belomorian Complex of the KC (e.g., *Lobach-Zhuchenko* et al., 1993). According to structural and seismic data the TB is a 5–12 km thick listric shear zone verging to the south with angles that decrease systematically from 60° to 10–12 ° along the listric structure (e.g., *Marker*, 1990, 1991; *Mints* et al., 1996; *Pozhilenko* et al., 1997). Numerous isotopic data on rocks from the eastern Tanaelv (Kolvitsa-Kandalaksha section) suggest its formation over an extended period ranging from about 2.5 to 1.9–1.85 Ga (e.g., *Mitrofanov* et al., 1993; *Glebovitskii* and *Efimov*,

* Abbreviations and symbols used in this paper are given in Appendix 1

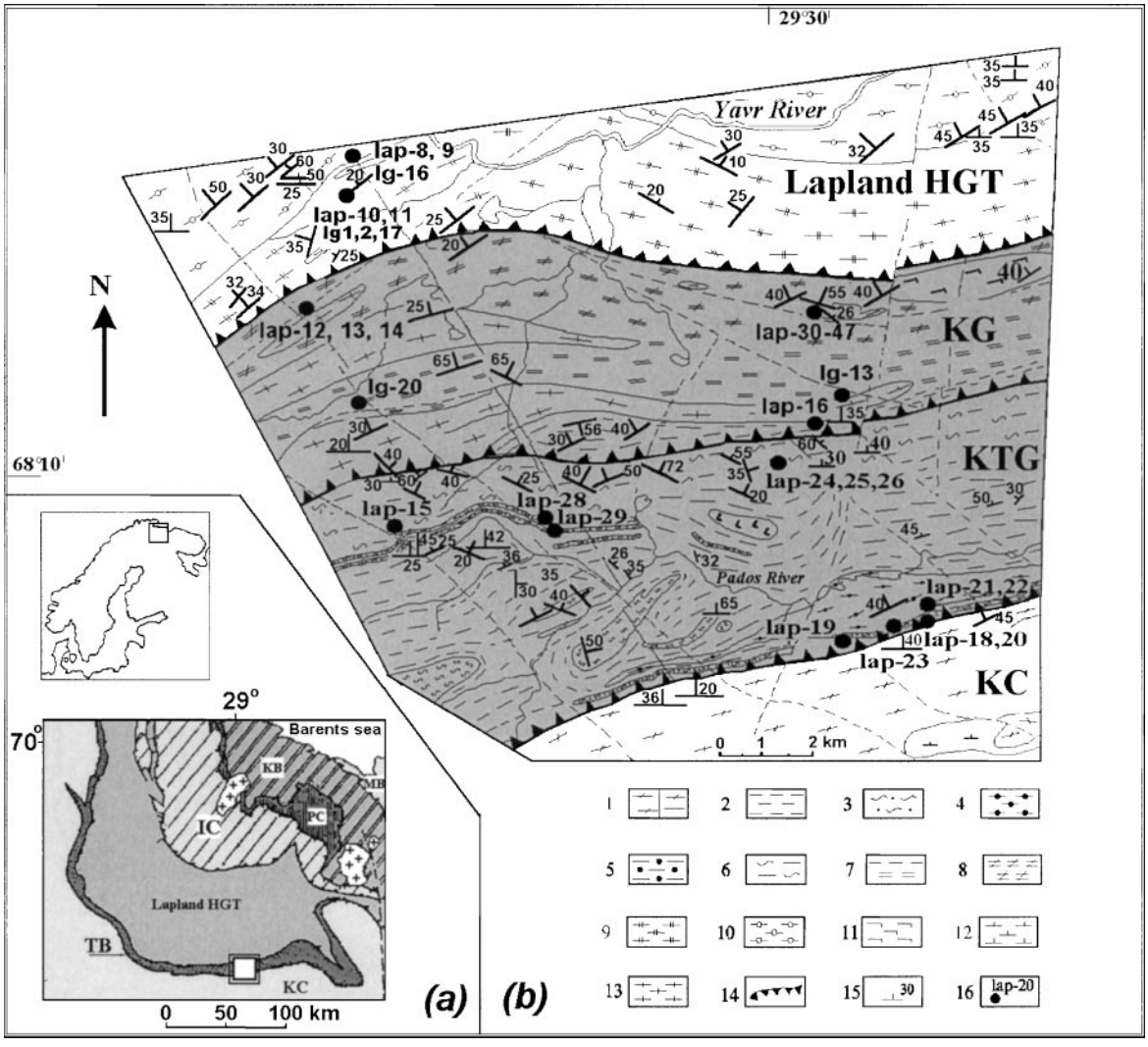

Fig. 1. Main tectonic units in the Northern Baltic shield (**a**) and geological map of the Pados-Yavr portion of the TB (**b**). **a** White rectangle on TB corresponds to map **b**; for abbreviations see Appendix A1-2. **b** Northern part of the **KC** (Belomorian Complex): 1 = biotite-amphibole gneiss. **KTG** (chlorite-staurolite and biotite-kyanite zones): 2 = chlorite-staurolite-garnet-muscovite and staurolite-biotite schists; 3 = biotite-muscovite-garnet-kyanite-plagioclase schists; 4 = schistose amphibolites; 5 = garnet gneisses; 6 = biotite and two-mica gneisses. **KG**: 7 = amphibole-biotite gneiss; 8 = garnet amphibolites and garnet-clinopyroxene amphibolites. **Lapland HGT**: 9 = basic granulites (garnet-pyroxene, pyroxene-plagioclase, and two-pyroxene schists and gneisses); 10 = silicic granulites (garnet-biotite gneiss with sillimanite); 11 = anorthosite; 12 = metaultramafic rocks; 13 = plagiogranite; 14 = deep thrusts; 15 = strike and dip symbols; 16 = sample localities

1997). *Benard-Griffiths* et al. (1984) obtained an age of 1.9 Ga for the western part of the TB in Fennoscandia. *Volodichev* (1990, p. 221) reported an age of 1.91 Ga for mica schists, and noted that these schists are confined to the Belomorian Complex that tectonically underlies the Lapland HGT. Isotopic data indicate that granulites of the Lapland HGT have a similar age of 1.9 Ga (e.g., *Mints* et al., 1996). The rocks of the Belomorian Complex, which tectonically underlie the Lapland granulites and the Tanaelv schists, are significantly older, 2.86–2.58 Ga (e.g., *Volodichev*, 1990; *Przhjialgovsky* and *Terekhov*, 1995). Therefore metamorphism of the Korva Tundra Group (KTG) mica schists of the TB (e.g., *Latyshev*, 1967, 1971; *Kozlov* et al., 1990; *Mints* et al., 1996) is synchronous with the formation of the Lapland granulite complex (e.g., *Bibikova* et al., 1993).

A well preserved temperature zonation across the TB is recorded in the paragenesis of garnet amphibolites, biotite-garnet gneisses, and mica schists (e.g., *Barbey* and *Raith*, 1990; *Fonarev* et al., 1994). Figure lb shows the systematic north directed change in the metamorphic grade from mica schists and epidote-garnet amphibolites of the KTG via the Kandalaksha group (KG) garnet amphibolites toward the Lapland HGT.

Hout River Shear Zone

The Southern Marginal Zone (SMZ) of the Limpopo HGT is characterized by large thrust sheets, 50 km by 20 km, of migmatitic granulites that display complex fold patterns designated as the early Dl phase of deformation (*Smit* and *van Reenen*, 1997). This early Dl event is also expressed as a thin-skinned system of northward verging low-angle thrusts on the adjacent KVC (*Roering* et al., 1992b). The thrust sheets in the SMZ are bounded by a system of km wide anastomosing ductile shear zones of the later D2 event of which the HRSZ is the largest (Fig. 2). The regional northward verging thin-skinned thrust system (Dl) of the northern Kaapvaal Craton (KVC) is therefore dramatically influenced by the superimposition of this major southward verging fault system (D2), giving rise to a distinct pattern of structural discontinuities (*Smit* and *van Reenen*, 1997).

The HRSZ is a composite structure, up to 5 km wide (*Smit* et al., 1992; *Smit* and *van Reenen*, 1997), which separates the Limpopo HGT from the adjacent greenstone terrains of the KVC. The HRSZ has been mapped as individual segments over a distance of more than 200 km bounding the SMZ in the south (*Roering* et al., 1992a,b). The HRSZ consists of E-W trending, steeply northward dipping thrusts and several near vertical NE trending strike slip faults. The strike slip faults acted as transfer zones linking the different thrust segments to form a zig-zag pattern of lateral and frontal ramps (*Perchuk* et al., 2000).

Detailed geo-electrical and seismic reflection data across the HRSZ (*de Beer* and *Stettler*, 1992), confirmed the suggestion (e.g., *de Wit* et al., 1992b; *Roering* et al., 1992a,b) that high grade rocks of the SMZ were thrusted southwards over low grade rocks of the KVC along the HRSZ. Geothermobarometric studies likewise showed that the vertical displacement across this crustal boundary was in the order of 15 km (*Miyano* et al., 1990; *Perchuk* et al., 1996).

Geological aspects related to the HRSZ is a subject of many studies (*van Schalkwyk* et al., 1987; *Miyano* et al., 1990; *van Reenen* et al., 1990; *de Wit* et al.,

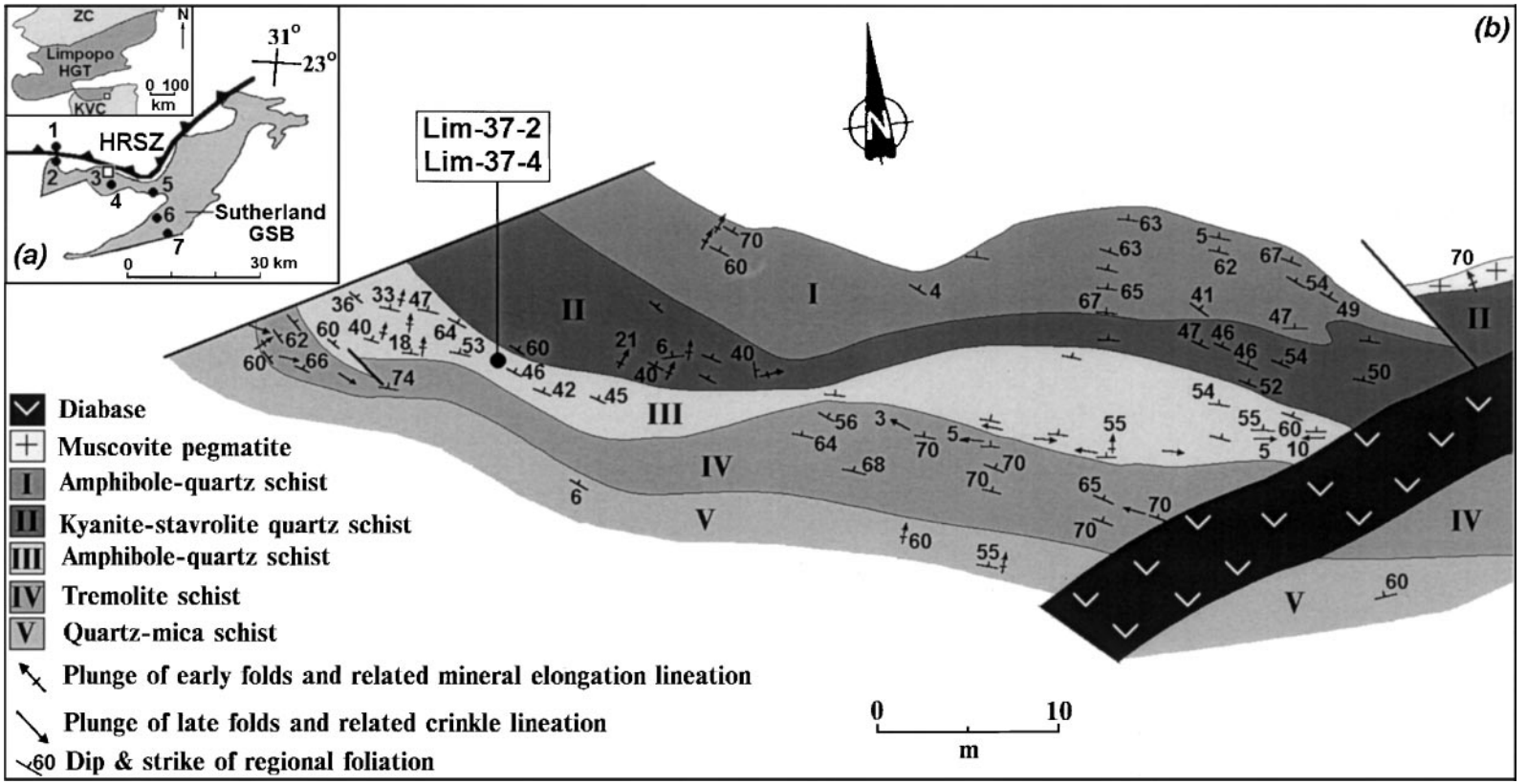

Fig. 2. **a** Geological position of an outcrop located in the HRSZ that separates the SMZ of the Limpopo Belt from the Sutherland greenstone belt of the Kaapvaal craton (see also Fig. 1b in *Perchuk* et al., 1999) **b** Detailed geological map of the River section east of the Klein Letaba Gold Mine (*McCourt* and *van Reenen*, 1992). Solid circles with numbers in maps a and b show localities, from which the samples (1) = G89-43, (2) = G89-10, G89-22, (3) = Lim-37-2, Lim-37-4, (4) = SL-22, K4, K5, K12, (5) = Lim-45, (6) = Lim-49, (7) = Lim-50 were collected

1992a,b; *McCourt* and *van Reenen*, 1992; *Roering* et al., 1992a,b; *Smit* et al., 1992; *Tsunogae* et al., 1992; *van Reenen* and *Smit*, 1996; *Kreissig* and *Holzer*, 1997; *Smit* and *van Reenen*, 1997) that mainly focussed on the emplacement mechanism of HGT between adjacent the Inari and Karelian cratons.

Figure 2b illustrates a small part of the HRSZ separating the Limpopo Belt from the Sutherland greenstone belt. The greenstone units on the KVC were mapped as large terrains metamorphosed from greenschist to amphibolite grade. The rocks of these terrains are faulted and rotated into concordance with the steeply northward dipping terrain boundary. In the SMZ of the Limpopo HGT greenstone assemblages were found occurring as intensely deformed and highly attenuated lenses in a mass of granitoid gneisses and migmatites (Fig. 1 in *Perchuk* et al., 1999). Highly sheared lithologies from the HRSZ that overlies the greenstone lithologies of the KVC and underlies the high-grade lithologies of the Limpopo HGT are representative of typical granite-greenstone lithologies of the KVC (*McCourt* and *van Reenen*, 1992; *Kreissig* and *Holzer*, 1997).

During the exhumation of the Limpopo HGT the 15 km vertical displacement across the HRSZ was associated with significant vertical displacement along smaller D2 shear zones within the granulite sub-zone of the SMZ. High grade rocks were therefore thrusted over low grade rocks of the craton, producing retrograde metamorphism in the SMZ and prograde metamorphism on the KVC along the terrain boundary.

Isotopic ages of the KVC vary between 2.9–3.5 Ma (*de Wit* et al., 1992a). Isotopic ages for the HRSZ have, however, only recently been produced by *Kreissig* and *Holzer* (1997). Synkinematic kyanite which developed in a highly sheared plagioclase-biotite-quartz-kyanite greenstone rock adjacent to the SMZ granulites was dated (Pb stepwise leaching method) at 2689 ± 7 Ma while monazite from pelitic granulites was dated at 2691 ± 4 Ma (*Kreissig* and *Holzer*, 1997). The two ages indicate that the formation of this fault system and the emplacement of granulites of the SMZ are isochronic.

Petrography

The Tanaelv Belt

The KTG mica schists (Fig. 1b) are in direct contact with Belomorian gray gneisses (Fig. 1b). Two metamorphic zones, chlorite-staurolite and kyanite-biotite , are distinguished in the KTG metapelites. The chlorite-out isograd coincides with the kyanite-in isograd. However chlorite occurs as inclusions in garnet porphyroblasts of the kyanite-biotite schist. The mineral assemblages of these rocks are shown in Table 1, sample locations in Fig. 1b.

Chlorite-staurolite zone. The schistose fabric of the rocks is complicated by microfolding while the texture is porphyroblastic with a schistose groundmass. Mineral modes vary considerably (in volume %): *St* = 5–20, *Chl* = 4–15, *Qtz* = 15–30, *Pl* = 15–40, *Ms* = 4–15, *Grt* = 5–15, *Bt* = 5–7, *Mag*, *Ilm*, and *Ep*, less than 3–4%. Small grains of kyanite, not in contact with biotite, were found in the matrix while rotated garnet porphyroblasts up to 12 mm in diameter (Fig. 3, Lap-20) with numerous inclusions of quartz, epidote, an opaque mineral, occasional biotite,

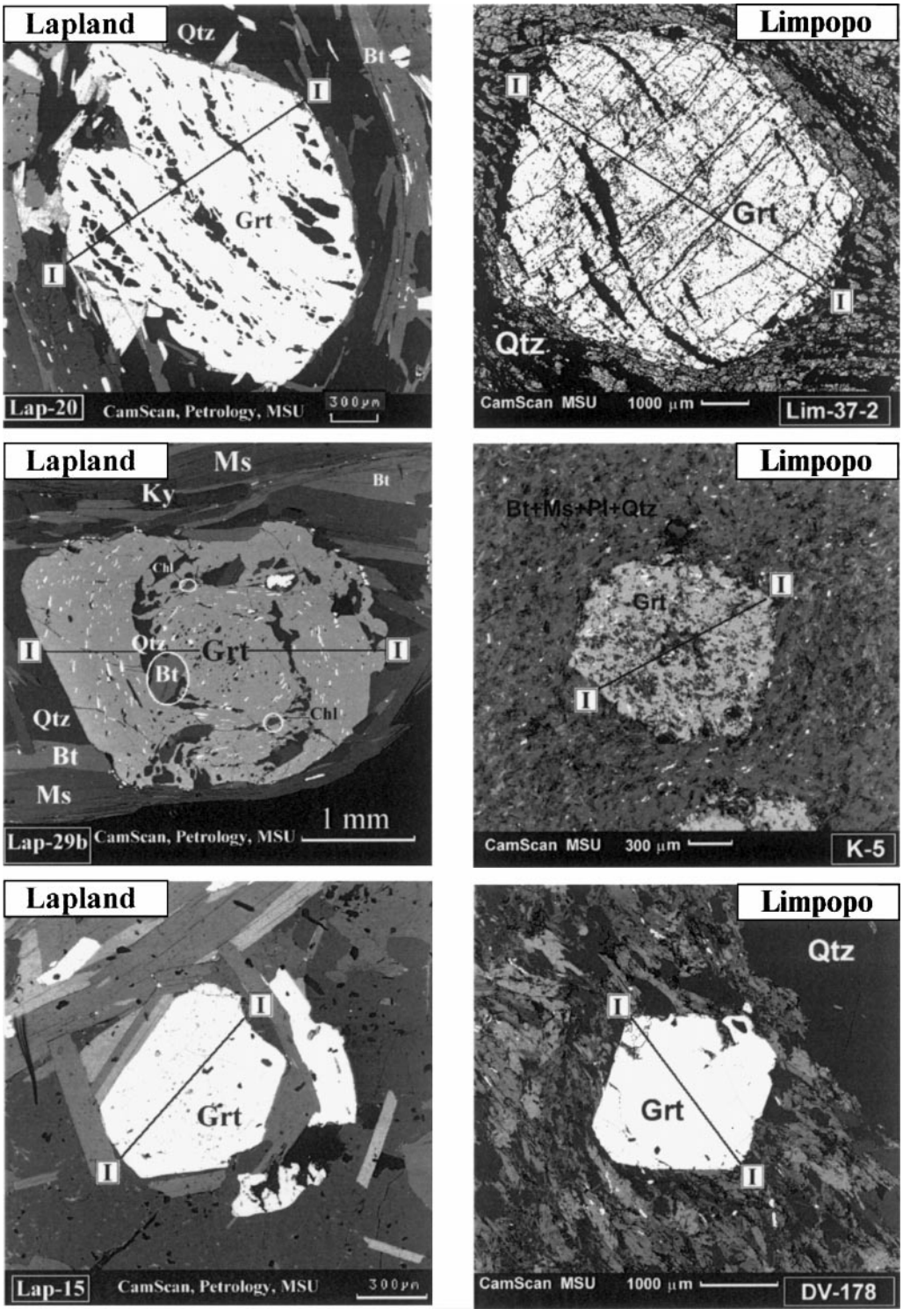

Fig. 3. Morphology of garnet porphyroblasts from the southern margins of the Lapland (TB) and Limpopo (HRSZ) complexes (see Table 1, and Figs. 1, 2). Detailed microprobe analyses have been performed along lines I-I. Back-scattered electron images by CamScan

muscovite, and staurolite were observed. Small irregular and inclusion-free garnets are rare. The garnet porphyroblasts are also surrounded by chlorite and mica aggregates while chlorite plates rarely occur as inclusions in garnet and staurolite. Staurolite usually occurs as irregular grains extensively replaced along margins and fractures by the secondary $Chl + Ms + Mag$ aggregates. In some of the samples large, up to a few centimeters in length, euhedral staurolite with quartz inclusions was observed while staurolite also occurs as inclusions in other minerals. Large, up to 10 mm in size, plagioclase contains inclusions of quartz, biotite, muscovite, and staurolite usually oriented in the same direction (sometimes at an angle to the schistosity) while small, inclusion-free plagioclase is also present. Foliated muscovite, chlorite and biotite aggregates define the weakly developed schistose structure. These minerals are also preserved as individual plates in large plagioclase and garnet grains. However, the biotite inclusions in the garnet porphyroblasts are very rare. In some thin sections, occasional small euhedral kyanite was observed in muscovite aggregates. Staurolite is common among biotite aggregates. Epidote occurs solely as rounded or elongated inclusions in garnet porphyroblasts.

The transition from the chlorite-staurolite zone to the kyanite-biotite zone is clearly demonstrated in a sample of a two-mica schist, Lap-24 (Table 1). This schist consists of (in volume %) $Qtz = 20–25$, $Pl = 10–15$, $St = 15–25$, $Bt < 1$; $Grt = 10–20$, $Ms = 20–30$, and $Chl = 2–3$. The schistose structure is complicated by microfolding. Large, up to 15–20 mm in diameter rotated garnet porphyroblasts with complex shapes contain spiral trails of quartz, biotite, muscovite, and staurolite inclusions. In the inner zone of the porphyroblasts, inclusions account for about 80% of garnet by volume while the outer zones are more homogeneous. Staurolite forms large crystals, crystal intergrowth, and inclusions in garnet. Rare chlorite occurs as plates in garnet. Kyanite is rare and occurs as individual small euhedral grains in muscovite aggregates. Inclusions of staurolite in garnet porphyroblasts are rather abundant and often euhedral. Staurolite is missing in the central parts of these garnet porphyroblasts, where quartz inclusions are abundant occurring only in the outer, optically homogeneous zones of garnet. Apart from sample Lap-24 (Table 1) no staurolite inclusions were observed in garnet porphyroblasts from the rocks of the KTG.

Kyanite-biotite zone. The mineral modes of the rocks from the kyanite-biotite zone are highly variable (in volume %): $Ky = 5–20$; $Qtz = 10–40$; $Pl = 3–20$; $Ms = 8–40$; $Grt = 5–20$; $Bt = 5–15$; $St = 5–7$; *Mag*, *Ilm* and $Ep = 3–4$. These rocks

Fig. 3 (*continued*)
electron microscope at the Department of Petrology, Moscow State University. *Rotated* garnet porphyroblasts (Lap-20 and Lim-37-2) were collected from the chlorite-staurolite zone of the TB and the HRSZ. The porphyroblasts mainly indicate a prograde stage of metamorphism. *Isometric* inclusion-rich garnet porphyroblasts (Lap-29b and K5) from the biotite-kyanite zone of the TB and the HRSZ indicate both prograde and retrograde stages of metamorphism. *Euhedral* inclusions-free garnet porphyroblasts (Lap-15 and DV-178) are taken from the chlorite-staurolite zone of the TB and the HRSZ. The porphyroblasts mainly indicate peak and retrograde stages of metamorphism

Table 1. *Mineral assemblages of sheared rocks from the Tanaelv Belt (Lapland) and the Hout River Shear Zone (Limpopo)*

Sample	Rock	Zone	Mineral assemblage*
		The KTG of the Tanaelv Belt (Kola Peninsula)	
Lap-19-3	Amphibolite	**Chl-St**	*Hbl + Grt + Bt + Ep + Qtz*
Lap-19-7	Amphibolite	**Chl-St**	*Hbl + Grt + Bt + Ep + Qtz*
Lap-19-5	Mica schst	**Chl-St**	*Qtz + Pl + St + Grt + Bt + Ms + Chl + Mag + Ilm + Ep*
Lap-19-8	Mica schst	**Chl-St**	*Qtz + Pl + St + Grt + Bt + Ms + Chl + Mag + + Ilm + Ep*
Lap-19-9	Mica schst	**Chl-St**	*Qtz + Pl + St + Grt + Bt + Ms + Chl + Mag + Ilm + Ep*
Lap-18-1	Mica schst	**Chl-St**	*Qtz + Pl + St + Grt + Ms + Chl + MagEp*
Lap-18-2	Mica schst	**Chl-St**	*Qtz + Pl + St + Grt + Ms + Chl + Mag + Ilm + + Ep*
Lap-20	Mica schst	**Chl-St**	*Qtz + Pl + St + Grt + Bt + Ms + Chl + Mag + + Ilm + Ky*
Lap-24	Mica schst	**Bt-Ky**	*Qtz + Pl + St + Grt + Ms + Chl + Mag + Ilm + + Ky*
Lap-15	Mica schst	**Bt-Ky**	*Qtz + Pl + St + Grt + Ms + Chl + Mag + Ilm + + Ky*
Lap-25	Mica schst	**Bt-Ky**	*Qtz + Pl + St + Grt + Ms + Chl + Mag + Ilm + + Ky*
Lap-28	Mica schst	**Bt-Ky**	*Qtz + Pl + St + Grt + Ms + Chl + Mag + Ilm + + Ky + Ep*
Lap-29	Mica schst	**Bt-Ky**	*Qtz + Pl + St + Grt + Ms + Chl + Mag + Ilm + + Ky*
Lap-29b	Mica schst	**Bt-Ky**	*Qtz + Pl + St + Grt + Ms + Chl + Mag + Ilm + + Ky*
		The KG of the Tanaelv Belt (Kola Peninsula)	
Lap-12	Amphibolite		*Hbl + Grt + Cpx + Bt + Pl + Qtz + Ilm*
Lap-13	Amphibolite		*Hbl + Grt + Cpx + Grt + Pl + Qtz + Ilm + Zrc*
Lap-14	Amphibolite		*Hbl + Grt + Cpx + Pl + Qtz + Ep + Ilm + Sph + Bt + Zrc*
Lg-13	Amphibolite		*Hbl + Grt + Pl + Qtz + Ep*
Lap-20	Amphibolite		*Hbl + Grt + Pl + Cpx + Qtz + Ilm + Zrc + Sph + Ap*
		The HRSZ (Limpopo)	
Lim-37-2	Amphibolite		*Grt + Ant + Hbl + Pl + Qtz + Bt*
Lim-37-4	Amphibolite		*Hbl + Pl + Qtz*
Lim-50	Amphibolite		*Hbl + Ep*
Lim-49	Amphibolite		*Hbl + Pl + Qtz*
G89-43	Amphibolite		*Hbl + Pl + Qtz*
G89-10	Amphibolite		*Act + Pl*
G89-22	Amphibolite		*Act + Pl + Qtz*
K12	Amphibolite		*Hbl + Pl + Qtz*
Lim-45	Chl schist		*Grt + Chl + Pl + Qtz*
K4	Mica schist		*Grt + Bt + Ms + Qtz + Pl*

(continued)

Table 1 (*continued*)

Sample	Rock	Zone	Mineral assemblage*
K5	Mica schist		$Grt + Bt + Ms + Qt + Chl + Pl$
SL22	Mica schist		$Grt + Bt + Ms + Pl + Qtz$
DV178	Mica schist		$Grt + Ged + Bt + St + Tur + Pl + Qtz$

*Probe analyses are available by e-mail: llp@geol.msu.ru

are, in many respects, similar to the schists of the chlorite-staurolite zone. Garnet forms porphyroblasts of various shapes and sizes (up to 10 mm). The inner parts of the porphyroblasts contain numerous inclusions of quartz, biotite, muscovite, chlorite, and staurolite, while the outer parts are inclusion-free. This indicates that growth of the porphyroblasts took place at different stages of metamorphism. In addition, small grains of irregular inclusion-free garnet also occur. Kyanite, of which there are two generations, contains plagioclase, quartz, muscovite, and magnetite inclusions. The first generation forms resorbed elongated grains trending parallel to the schistosity of the rock. They are almost devoid of crystal faces and form intergrowths with white mica. This kyanite probably formed during the prograde stage of metamorphism while retrograde kyanite of the second generation forms large crystals, up to a few centimeters in diameter, cross-cutting mica aggregates show perfect crystallographic habits. Staurolite forms elongated crystals oriented parallel to the schistosity. Occasional inclusions of chlorite occur in the staurolite and garnet porphyroblasts. Chlorite also appears around garnet and kyanite in association with micas. In some mica aggregates the relict chlorite is replaced by biotite. Biotite and muscovite form a foliated aggregate defining the schistose structure of the rock. In most cases, more euhedral muscovite is distinctly predominant in the aggregate. Biotite also occurs as large, up to 400 microns inclusions in garnet porphyroblasts. Plagioclase contains parallel inclusions of quartz, muscovite, biotite, staurolite, and an opaque mineral.

It is concluded that the KTG (Fig. lb) is composed of two prograde metamorphic zones: chlorite-staurolite and kyanite-biotite. The first zone tectonically overlies the gneisses of the BC (KC) while the second zone is also in tectonic contact with the garnet amphibolites of the KG. In the samples from the kyanite-biotite zone, chlorite is either absent or present as rare inclusions in garnet and (or) staurolite. Except for the above-mentioned cases, kyanite does not occur in the chlorite-staurolite zone.

Hout River Shear Zone

Table 1 shows the wide spectrum of mineral assemblages composing the HRSZ. They range from typical metapelites ($Bt + Mu + Chl + Qtz + Pl \pm Grt$) to typical amphibolites ($Hbl + Pl + Qtz \pm Grt$). Reaction textures were never observed but the rocks are characterized by a variety of microstructural elements such as microschistosity, lineations, syn- and post-deformational porphyroblasts, and the presence of low- to high-strain micro zones. These microstructural elements are particularly well developed in mica schists.

A typical mica schist (samples SL22, K5, Table 1) is composed of (in volume %): Bt = 10–20%, *Ms* = 20–30%, *Chl* = 10–15%, *Qtz* = 25–35%, *Pl* = 5–10% and rare, but not secondary garnet $\sim$ 5%. Syn-deformational garnet porphyroblasts of different shapes and sizes are filled with quartz inclusions. The inclusions commonly show rotational traces and pressure shadow wings as kinematic indicators (Fig. 3, K5). Such features are, however, less prominent than in the schists of the TB (*Perchuk* and *Krotov*, 1998). In the garnet porphyroblasts the outer portions commonly show a regular crystallographic shape while inclusions are concentrated in the central portions of grains (Fig. 3, K5). Biotite porphyroblasts surrounded by small oriented high-strain biotite and muscovite crystals can also be found. Post-deformational flakes of mica seldom cross cut the schistosity plane. Plagioclase forms small inclusion-free grains in the matrix.

The garnet-bearing gneissic rocks also contain amphibole-bearing varieties (e.g. Lim-37-2 and DV-178, Table 1). Two types of garnet, very similar to those in TB, are prominent in these rocks (Fig. 3). The first type is represented by large, up to 10–15 mm in diameter syn-deformational rotated garnet porphyroblasts containing spiral trails of quartz and amphibole inclusions (Fig. 3, Lim-37-2). The second type occurs as relatively small inclusion-free post-deformational grains commonly with regular crystallographic shapes and without pressure shadows (Fig. 3, DV-178). The composition of these garnets commonly corresponds to the outer zones of syndeformational garnet porphyroblasts.

Two stages of deformation and mineral growth

The Tanaelv Belt

Two major types of garnet porphyroblasts are observed in mica schists of the TB (*Perchuk* et al., 1996; *Perchuk* and *Krotov*, 1998). The first type, characterized by rotated garnets, occurs only in rocks of *the chlorite-staurolite zone* of the TB (Fig. 1) and in the HRSZ (Fig. 2). It is represented by garnet porphyroblasts with numerous inclusions of quartz, epidote, and titanomagnetite. These inclusions occur as ribbon forms outlined by sub-parallel S-shaped quartz trails (Fig. 3, Lap-20). Inner and outer zones are clearly recognized in the structure of all of the porphyroblasts and are related to different deformational episodes. In the inner zone inclusions normally form curved parallel trails oriented at an angle to the schistosity of the rock. The trails are bent toward the outer zones and parallel to the contour of the porphyroblast. Many large porphyroblasts show proper euhedral or sub-euhedral shapes and elements of crystal faces. Each of the samples is characterized by a particular porphyroblast morphology and distribution of inclusion in the porphyroblasts. For instance, the porphyroblasts of sample Lap-19/9 (Table 1) contain inclusions of quartz and less abundant euhedral crystals of staurolite, muscovite, chlorite, an opaque mineral, and epidote. The inclusions form complicated contorted trails and in some portions of the porphyroblasts, such trails are oriented at an angle to the majority of other trails, including a perpendicular orientation. Porphyroblasts with clearly defined inner zones also occur in this sample. The inner zone contains abundant inclusions of the above-

mentioned minerals, whereas the outer zone is essentially inclusion-free. The second generation of garnet occurs more often in the kyanite-biotite zone of the TB (Fig. 3, Lap-15). These porphyroblasts always show clearly defined euhedral outlines. They contain a very small amount of inclusions of quartz and opaque minerals randomly distributed within the euhedral grains while some porphyroblasts are completely devoid of inclusions. The complimentary textural characteristics of the porphyroblasts and phyllosilicates of the matrix suggest that recrystallization of the rock proceeded under decreasing *P-T* metamorphic conditions. In other words, deformation associated with the retrograde metamorphic stage is essentially not manifested in these rocks.

Snow-ball garnets were sometimes observed with prograde and retrograde porphyroblasts in some samples of mica schists from the KTG of the TB, Kola Peninsula (Fig. 3, Lap-29b). Normally these garnets show flat N_{Mg} patterns that reflect peak metamorphic conditions (*Perchuk* and *Krotov*, 1998). Similar patterns were found in garnet amphibolites of the HRSZ. Epidote amphibolites and garnet amphibolites that intercalate with mica schists of the KTG (Fig. 1b) never contain rotated or snow-ball garnet. However chemical zoning of euhedral porphyroblasts from these rocks demonstrate prograde and retrograde chemical zoning identical to that observed in mica schists.

Hout River Shear Zone

The garnet porphyroblasts of the HRSZ that adjoins the Limpopo complex in the south preserve an inverse chemical zonation in terms of N_{Mg} and N_{Ca} (Fig. 3, Lim-37-2 and K-5). The formation of this inverse zonation is accompanied by crystallization of two generations of biotite, reflecting the prograde and retrograde stages of the *P-T* evolution of the schists. In addition, the prograde zone in the garnet porphyroblasts is characterized by the presence of oriented inclusions of different minerals, while the retrograde zone is inclusion-free. In some mica schists the idiomorphic garnet porphyroblasts (*Grt1*) are wrapped by the fine-grained schistose matrix composed of chlorite, muscovite and biotite. The inclusion-rich garnet core is surrounded by an inclusions-poor zone with idiomorphic facets (e.g., SL-22, Table 1). The outer zone is similar in composition to matrix *Grt2* and definitely grew during the post-deformational stage. In several cases evidence for brittle deformation of both *Grt1* and *Grt2* suggests intensive shearing of the rocks during the late retrograde stage (e.g., Lim-37-2, Table 1).

Thus, in both the TB and the HRSZ some porphyroblasts of minerals such as garnet, kyanite, staurolite, etc. reflect the presence of two generations suggesting different stages of growth in the two studied shear zones. The syn-deformational growth of the rotated garnet porphyroblasts and phyllosilicates was followed by the formation of post-peak inclusion-free euhedral garnet. Thus, using microtextural indicators, syn- and postkinematic mineral growth that correlates with the prograde and retrograde stages of metamorphism of the rocks can clearly be distinguished. The majority of workers (e.g., *Hörmann* et al., 1980; *Raith* et al., 1982; *Barbey* and *Raith*, 1990; *Daly* and *Glbovitskii*, 1991; *van Reenen* and *Smit*, 1996) reached similar conclusions. The textural data are supported by data on chemical zoning of the garnet porphyroblasts (Fig. 4).

Mineral chemistry

Apparatus and methods

Optically examined thin sections were investigated with a scanning electron microscope (*CamScan-Cambridge*) in the Department of Petrology at Moscow State University, and with a Cameca microprobe in the Department of Geology at the Rand Afrikaans University, both equipped with an energy-disperse Link system. Almost 3000 analyses were obtained, the majority of which are from garnet porphyroblasts. Microprobe line scans, with 30–60 μm steps, were obtained from garnet porphyroblasts from almost all of the samples listed in Table 1. The analyses of hydrous minerals were recalculated to cation fractions (tentative crystallo-chemical formulas) using the oxygen method: 22 oxygens for micas, 28 for chlorites, 11 for staurolites, and 12 for epidotes. Following other researchers, e.g., *Laird* (1991), all iron was recalculated as ferrous iron which appeared to be quite reasonable as the tentative formulas of water-bearing Fe-Mg minerals showing rather stable cation sums.

The Tanaelv Belt

About 2000 analyses of coexisting minerals were done in order to estimate the *P-T* evolution of metamorphism in the TB (*Perchuk* and *Krotov*, 1998). A thorough knowledge of the major kind of isomorphic substitution in each mineral is crucial in utilizing the methods of mineral thermobarometry (*Perchuk*, 1990; *Perchuk* and *Lavrent'eva*, 1983). Line scans for Mg, Ca, and Mn across porphyroblasts of Fig. 5 demonstrate the extensive $(Mg + Fe) \rightleftharpoons Mn$ substitution, especially in the cores and near the rims of grains. An increase in N_{Mg}^{Grt} toward the rims of grains is predominant. This particular isomorphic substitution is typical for garnet porphyroblasts from the *chloritestaurolite zone* of the KTG (e.g., Figs. 1b, 3 and 4). In some garnets from the *kyanite-biotite* zone of the KTG prograde and retrograde metamorphic stages are only slightly reflected by mineral zoning.

In the KTG of the TB N_{Mg} of biotite and other hydrous minerals, namely chlorite, staurolite, muscovite, and epidote varies negligibly, not only in individual samples, but also within each metamorphic zone (*Perchuk* and *Krotov*, 1998). Biotite of the prograde and retrograde stages similarly shows small variation in N_{Mg}^{Bt} but differs significantly in aluminum content. The average value of $Al^{VI} + Al^{IV}$ is 3.29 for the prograde, and 3.65 and 3.62 for peak and retrograde biotites, respectively. Muscovite contains a maximum of 8 mole % of the celadonite component. The N_{Mg}^{Chl} of inclusions in the garnet porphyroblasts from the kyanite-biotite zone increases by 3–4 mole % as compared with those from the chlorite-staurolite zone due to Fe-Mg exchange with garnet. A biotite inclusion 400 μm long was found in a snowball garnet with N_{Mg} of garnet around *Bt* only varying within 18–17 mole % as is demonstrated by a microprobe line scan across the biotite flake at a step of 50 microns:

Data point	*Grt-1*	*Bt-42*	*Bt-43*	*Bt-44*	*Bt-45*	*Bt-46*	*Bt-47*	*Bt-48*	*Bt-49*	*Bt-50*	*Grt-51*
N_{Mg}, %	17	56	57	58	57	59	58	58	58	57	17

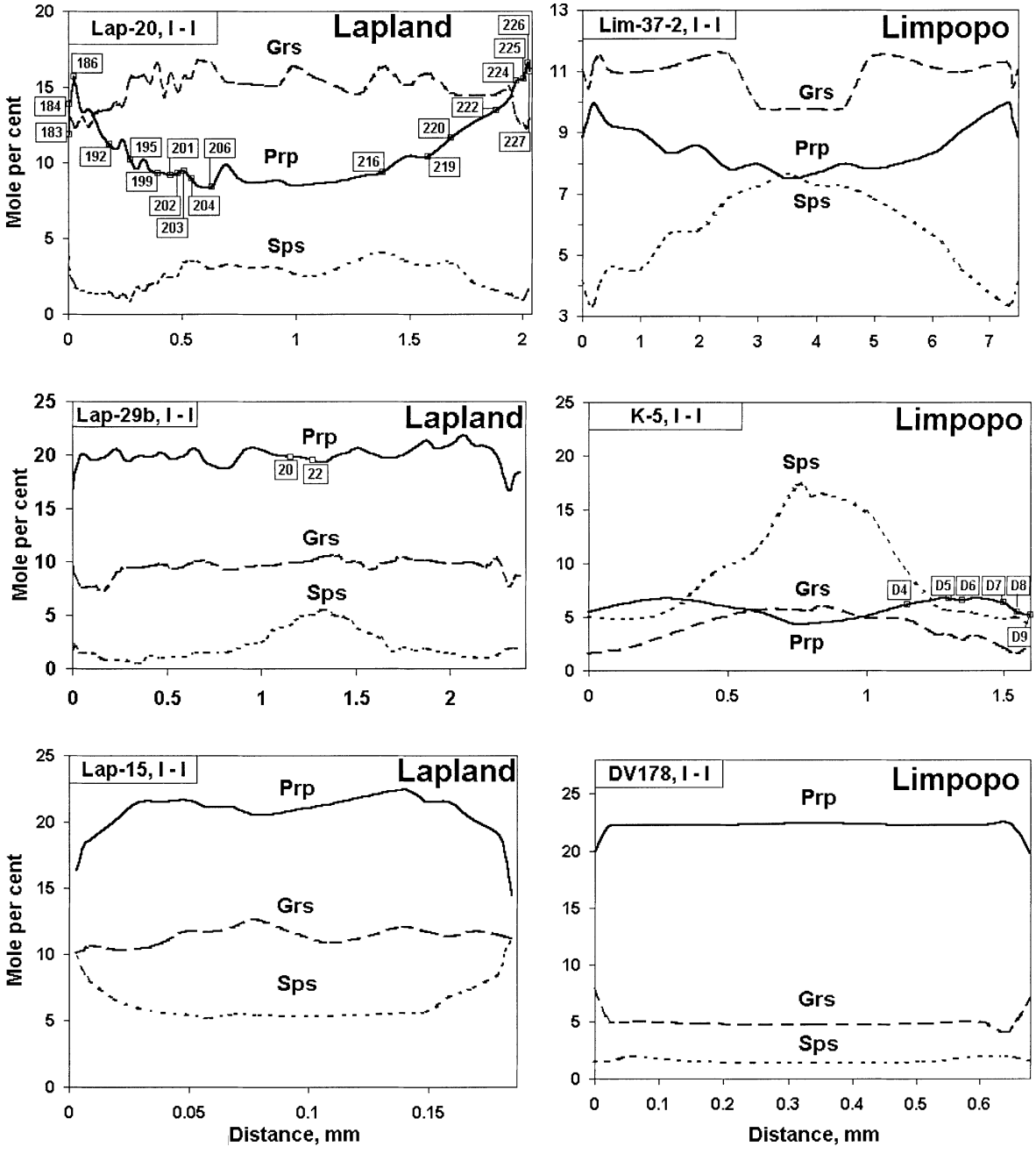

Fig. 4. Line scans across garnet porphyroblasts from sheared wall rocks (see Fig. 3) from the TB and HRSZ. The scans characterize prograde and retrograde stages of metamorphism

Such changes in biotite composition correspond to a temperature increase of approximately only 5 °C (*Perchuk*, 1990). A similar result was obtained from microprobe line scans across a 50 microns chlorite flake included in garnet (Sample Lap-29 b):

Data point	*Grt-88*	*Chl-106*	*Chl-107*	*Chl-108*	*Chl-109*	*Chl-110*	*Grt-111*
N_{Mg}, %	20	56	52	54	58	55	20

The composition of chlorite in contact with garnet is identical at the start and the end of the scan. This suggests an insignificant change in metamorphic temperature (*Perchuk*, 1990).

Hout River Shear Zone

A typical microprobe line scan from core to rim of the garnet porphyroblast in Fig. 4 (Limpopo) illustrates a dramatic decrease in N_{Mn}^{Grt} and in some samples (e.g., K5), also of N_{Ca}^{Grt} accompanied by an inverse change in N_{Mg}^{Grt}. Both garnet generations differ in composition and in the details of the microprobe scans. Inverse correlation involving N_{Mg}^{Grt} reflects two successive stages of metamorphism, i.e. pre- or syn-deformational prograde and post-deformational retrograde metamorphic events. They are accompanied by two distinct structural generations of mica. Syn-deformational biotite (*Bt1*) is oriented parallel to the schistosity, while post-deformational biotite (*Bt2*) crosscuts the schistosity. N_{Mg} is about 31 for *Bt1*, and 31–36 for *Bt*2. *Bt1* also demonstrates a lower Al content than *Bt2*. Biotite with $N_{Mg} = 31.5$–33 associated with small garnet grains with $N_{Mg}^{Grt} = 5.4-4.4$, defines the latest stage of the metamorphic evolution of mica schists.

Thus, zoning of the garnet porphyroblasts and two mica generations in metapelitic rocks from the HRSZ of the KVC near the contact with the Limpopo granulite belt reflects both prograde and retrograde stages of regional metamorphism.

Prograde zoning was also described in garnets from amphibolites of the HRSZ (*Perchuk* et al., 1996). For example, large, up to 10 mm syn-deformational garnet in amphibolite Lim-37-2 (Fig. 3) is preserved in a clearly schistose matrix composed of common hornblende, anthophyllite, plagioclase and quartz. The banded texture of the rock is defined by the intercalation of *Hbl* and *Qtz-Pl* lenses reflecting low-strain zones. The syn-deformational origin of the rounded garnet porphyroblasts is supported by the presence of oriented *Hbl* inclusions, as well as by elongated block-inclusions of *Qtz-Pl.* The distribution of the inclusions within the porphyroblast mimics the texture of the rock. Pressure-shadow wings which surround garnet porphyroblasts are additional evidence for their syn-deformational growth. As was observed in metapelites (Table 1, SL22 and K5), amphibolite sample Lim-37-2 also demonstrates systematic distribution of inclusions in garnet porphyroblasts. The cores and inner zones of porphyroblasts are characterized by the presence of oriented inclusions, while the idiomorphic rims are inclusion-free. Microprobe line scans show a gradual decrease in N_{Mg}^{Grt} from 9 to 12 followed by a sharp decrease to $N_{Mg}^{Grt} = 10$ at the contact with rock matrix while N_{Mg}^{Hbl} varies within analytic error.

Thus, as often described in the literature (e.g., *Spry*, 1963; *Powell*, 1966, 1970; *Powell* and *Treagus*, 1967; *Rosenfeld*, 1970; *Schoneveld*, 1977; *Reinhard* and *Rubenach*, 1989; *Johnson*, 1993a,b; *Johnson* and *Bell*, 1996; *Perchuk* and *Krotov*, 1998) the composition and growth texture of garnet porphyroblasts from individual

samples may correspond to prograde or retrograde metamorphic stages. For example, both the rotation morphology and an increase in N_{Mg} (and a decrease of N_{Mn}) from core to rim of the garnet porphyroblast suggest prograde metamorphism (Fig. 3, Lim-37-2). Such garnets are interpreted as syn-tectonic porphyroblasts forming from a single nucleas during the prograde metamorphic stage, and preserved due to rapid movement of the rock in the *P-T* field in comparison with the solid-state diffusion rate or/and mineral growth.

Mineral reactions and metamorphic conditions

Mineral assemblages (Table 1) and the chemistry of garnet, micas, and chlorite allow the evaluation of the *P-T* history of the TB and the HRSZ. The method used to estimate mineral equilibria in the mica schists and to calculate the *P-T* parameters of their metamorphic evolution has been described in detail (*Gerya* et al., 1997; *Perchuk* and *Krotov*, 1998). This method is based on the evaluation of microstructural evidence for synchronous growth of minerals in certain mineral associations. For example, prograde rotated garnet porphyroblasts (Fig. 4) grew simultaneously with inclusion-rich staurolite and/or kyanite porphyroblasts. It is therefore expected that mineral inclusions in the cores will be in equilibrium with the host mineral, while the rim of the host mineral is in equilibrium with contact mineral(s). On the other hand, inclusion-free garnet porphyroblasts (e.g., Fig. 4, Lap-15 and DV-178) are expected to be in equilibrium with retrograde biotite, staurolite and/or kyanite.

The Tanaelv Belt

A temperature zonation across the SW margin of the Lapland complex (including the TB) was first described by *Barbey* and *Raith* (1990) who showed a systematic decrease in temperature from the central part of the complex to the adjacent cratons. Figure 5 demonstrates the temperature zonation calculated for cores of coexisting minerals using the *Bt-Grt*, *Hbl-Grt*, *Hbl-Cpx*, *Chl-Grt*, *Grt-St* etc. geothermometers (*Perchuk*, 1990). In Fig. 1b the metamorphic grade progressively increases northward, from the KTG epidote amphibolites and mica schists through the KG garnet amphibolites to the Lapland granulites. In combination with the geochronological data of *Bernard-Griffiths* et al. (1984), such a metamorphic zoning indicates that the formation and evolution of the mica schists of the Tanaelv belt were closely linked to the development of the Lapland granulite complex. Moreover, this zonation has been interpreted as a result of a thermal event caused by ascent of the Lapland granulite body (*Perchuk* et al., 1997). A detail study of schists from this area gave more information on the *P-T* evolutions within the TB (*Perchuk* and *Krotov*, 1998).

The most important associations from the KTG and KG (Fig. 1 and Table 1) are $Chl + St + Bt + Ms + Grt + Pl + Qtz + Mag$ for *the chlorite-staurolite zone* and $Ky + Bt + St + Ms + Grt + Pl + Qtz + Mag$ for *the kyanite-biotite zone*. The reaction

$$Chl + Ms + St \Rightarrow Ky + Bt + Qtz + H_2O \quad (1)$$

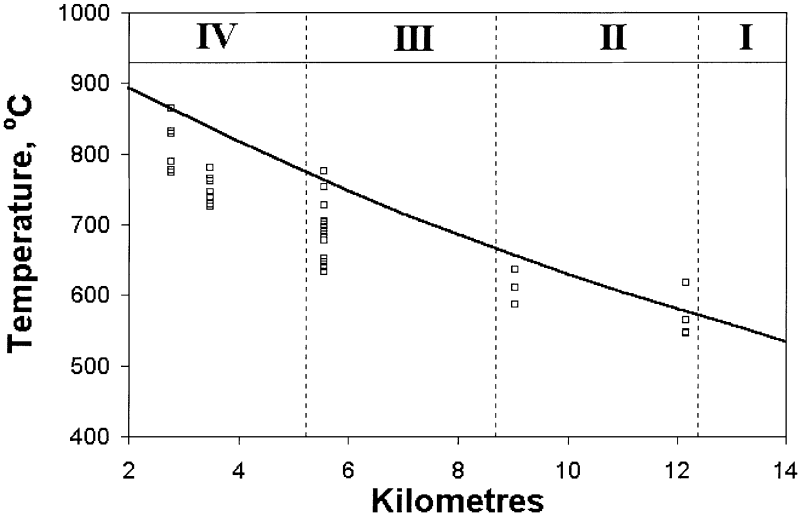

Fig. 5. Temperature zonation documented by geothermometry across the TB between the Lapland granulite complex and the Belomorian gneisses of the Karelian craton (see Fig. 1). Temperatures were calculated for cores of coexisting minerals using the *Bt-Grt*, *Hbl-Grt*, *Hbl-Cpx*, *Chl-Grt*, and *Grt-St* geothermometers (*Perchuk*, 1990). See text for discussion

defines the boundary between these two zones (e.g., *Carmichael*, 1970; *Hiroi*, 1983) in many metamorphic complexes of the kyanite-sillimanite type (*Miyashiro*, 1973). Reaction (1) shifts to the right with increasing temperature and pressure (Fig. 6). Both diagrams of Fig. 6 are conventional because garnet contains Mn, i.e. reaction (1) reflects the bi-variant equilibrium. This results in the wide spread occurrence of chlorite inclusions in garnet porphyroblasts and mica schists of the kyanite-biotite zone which is not accounted for in the schematic projection of Fig. 6b. On the other hand, the diagram of Fig. 6b shows identical Mg numbers for staurolite and garnet ($N_{\mathrm{Mg}}^{Grt} = N_{\mathrm{Mg}}^{Chl} = 23$) in the kyanite-biotite zone. The mineral assemblages of mica schists of the KTG allow a reliable estimation of the *P-T* parameters for the metamorphic evolution of the TB (*Perchuk* and *Krotov*, 1998) at the southern border of the Lapland granulite complex.

No significant difference was found between the *P-T* parameters obtained for mineral compositions of contacting minerals from the schist matrix and for the pair ''inclusion + garnet porphyroblast''. For instance, the following temperatures were calculated for rock sample Lap-19-8 (Table 1) using the latest version of the garnet-chlorite thermometer (*Perchuk*, 1989, 1990) without a correction for the Ca content of garnet:

Chlorite	Probe data point	N_{Mg}^{Grt}	N_{Mg}^{Chl}	T°C
Chl of matrix	*Grt*(21, core) + *Chl*(73, core)	11	66	450
Chl of matrix	*Grt*(04, margin) + *Chl*(75, rim)	16	65	500
Chl from the *Grt* porphyroblast	*Grt*(59, core) + *Chl*(62, core)	10	61	460
Chl from the *Grt* porphyroblast	*Grt*(54, margin) + *Chl*(53, rim)	14	67	483

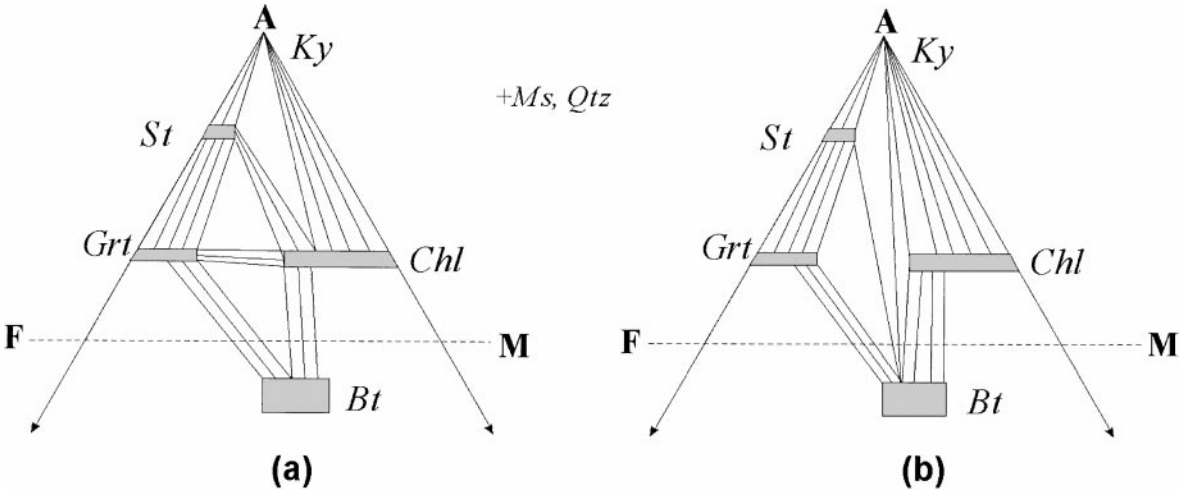

Fig. 6. Thompson's projections for the mineral paragenesis of mica schists from of the Korva Tundra Group of the TB. **a** chlorite-staurolite zone; **b** kyanite-biotite zone. Transition from zone (**a**) to zone (**b**) proceeds through the prograde reaction (1) (see text for further explanation)

In the first case, the composition of cores and rims of garnet is compared with that of chlorite from the micaceous matrix. In the second case, the compositions of the garnet core and rim are taken together with chlorite inclusions in direct contact with the host garnet. In both cases an increase in temperature is evident (chlorite-staurolite zone). In many cases, however, there were no need for such an approach, because the Mg number of biotite in an individual sample varies only within 2 mole %. As a result, the changing *P-T* parameters during the syn- and post-kinematic stages of schist metamorphism appeared to be essentially completely recorded in the garnet zoning. The same conclusion was reached by *Fonarev* et al. (1994).

Temperatures for the mica schists were calculated using the *Bt-Grt* thermometer (*Perchuk*, 1989, 1990) while pressures were obtained with an empirical *Ms-Qtz-Bt-Grt*-Al_2SiO_5 barometer (*Perchuk*, 1973, 1977) based on the reaction (see Appendix 2):

$$1/3Phl + 2/3Al_2SiO_5 + 1/3Qtz = 1/3Prp + 1/3Ms \qquad (2)$$

Perchuk and *Krotov* (1998) corrected this barometer with respect to experimental data on the *Bt-Grt* thermometer (*Perchuk* and *Lavrent'eva*, 1983) and thermodynamic data on the end-member properties in reaction (2).

The calculated *P-T* parameters of local mineral equilibria in the mica schists are given in Table 2. These data were used to construct a *P-T* path for the rocks studied. Figure 7 shows prograde (a) and retrograde (b) *P-T* paths for mica schists from the TB. According to eq. (A2, A3 in Appendix 2), both diagrams account for the Ca content of each of the garnet analyses. The metamorphic peak is defined at $T = 630\,^{\circ}C$ and $P = 7.3$ kbar. Figure 7a reflects the burial of schists to a depth of about 22 km, corresponding to chemical zoning of garnet in Fig. 4 (Lap-20) at negligible variations in N_{Mg}^{Bt} and N_{Ca}^{Grt}. Figure 7b shows the exhumation of the schists

Table 2. *Compositions of coexisting minerals and P-T parameters for the schists from the Tanaelv Belt (Lapland) and the Hout River Shear Zone (Limpopo)*

	*Grt**				*Bt**			*T*, °C	*P*, kbar
Spot	X_{Mg}	X_{Ca}	X_{Mn}	Spot	X_{Mg}	X_{Si}	X_{Al}		
The TB (Kola Peninsula)									
Lap-20 (*retrograde stage*)									
186	0.184	0.128	0.022	290	0.602	0.532	0.255	570	5.89
192	0.133	0.138	0.015	285	0.615	0.528	0.246	496	4.49
195	0.122	0.157	0.009	330	0.590	0.529	0.266	496	4.43
199	0.114	0.170	0.021	271	0.603	0.528	0.250	477	4.06
201	0.112	0.163	0.024	267	0.604	0.527	0.246	473	3.92
202	0.112	0.151	0.026	266	0.612	0.534	0.258	468	3.80
203	0.117	0.162	0.034	269	0.591	0.519	0.246	488	4.04
204	0.110	0.162	0.035	268	0.598	0.530	0.244	473	3.76
206	0.104	0.171	0.030	333	0.606	0.532	0.252	460	3.62
216	0.118	0.171	0.041	334	0.602	0.528	0.246	483	4.00
218	0.129	0.164	0.032	275	0.603	0.534	0.250	498	4.40
219	0.143	0.152	0.034	274	0.609	0.528	0.250	513	4.72
220	0.152	0.147	0.021	335	0.597	0.520	0.240	533	5.14
222	0.171	0.151	0.014	295	0.607	0.528	0.250	551	5.69
224	0.180	0.126	0.009	293	0.606	0.530	0.250	563	5.86
225	0.193	0.126	0.015	294	0.595	0.532	0.251	587	6.23
226	0.188	0.136	0.016	295	0.607	0.528	0.250	572	6.05
227	0.163	0.133	0.028	296	0.617	0.530	0.248	533	5.20
183	0.143	0.135	0.037	329	0.603	0.532	0.253	516	4.63
184	0.165	0.132	0.030	291	0.617	0.531	0.257	535	5.23
Lap-29b (*prograde stage*)									
22	0.207	0.107	0.051	55	0.584	0.533	0.264	612	6.28
20	0.207	0.104	0.040	56	0.569	0.532	0.260	625	6.50
75	0.211	0.108	0.040	45	0.573	0.537	0.257	627	6.58
73	0.212	0.104	0.035	46	0.591	0.502	0.250	613	6.48
94	0.141	0.085	0.028	95	0.564	0.531	0.258	539	4.62
88	0.192	0.094	0.021	98	0.567	0.537	0.260	607	6.24
51	0.177	0.094	0.020	50	0.587	0.523	0.256	572	5.66
54	0.206	0.096	0.020	49	0.583	0.538	0.262	612	6.49
41	0.187	0.089	0.020	110	0.555	0.363	0.248	610	6.19
Lap-15 (*prograde and peak stages*)									
161	0.229	0.120	0.056	76	0.610	0.534	0.259	617	6.58
162	0.237	0.101	0.045	77	0.602	0.523	0.248	633	6.89
165	0.241	0.128	0.022	129	0.601	0.530	0.257	640	7.29
166	0.239	0.132	0.018	130	0.605	0.534	0.254	634	7.25
167	0.236	0.128	0.017	131	0.603	0.531	0.252	632	7.20
169	0.231	0.131	0.013	152	0.605	0.534	0.257	625	7.11
172	0.229	0.134	0.013	153	0.603	0.532	0.257	624	7.09
175	0.236	0.145	0.017	154	0.598	0.531	0.254	637	7.30
177	0.231	0.131	0.017	187	0.612	0.541	0.261	619	7.01
178	0.237	0.132	0.019	189	0.617	0.538	0.261	621	7.09
182	0.224	0.138	0.035	186	0.602	0.534	0.258	619	6.79

(continued)

Table 2 (*continued*)

	*Grt**				*Bt**			*T*, °C	*P*, kbar
Spot	X_{Mg}	X_{Ca}	X_{Mn}	Spot	X_{Mg}	X_{Si}	X_{Al}		
Lap-15 (*retrograde stage*)									
157	0.151	0.124	0.130	72	0.585	0.539	0.262	537	4.07
158	0.173	0.132	0.094	73	0.606	0.532	0.250	552	4.92
159	0.207	0.125	0.075	74	0.589	0.522	0.243	607	6.07
160	0.212	0.132	0.072	75	0.613	0.532	0.256	594	6.05
184	0.174	0.154	0.083	185	0.596	0.543	0.268	561	5.18
The HRSZ (Limpopo)									
S1-22† (prograde stage)									
C22	0.059	0.052	0.085	C45	0.311	0.575	0.279	558	5.99
C23	0.065	0.046	0.083	C45	0.311	0.575	0.279	577	6.37
C24	0.074	0.036	0.074	C45	0.311	0.575	0.279	605	6.93
C25	0.069	0.043	0.071	C45	0.311	0.575	0.279	590	6.70
C26	0.067	0.045	0.079	C45	0.311	0.575	0.279	583	6.52
C18	0.068	0.042	0.058	C45	0.311	0.575	0.279	587	6.72
C19	0.065	0.039	0.062	C45	0.311	0.575	0.279	577	6.48
C20	0.061	0.045	0.075	C45	0.311	0.575	0.279	565	6.16
C21	0.064	0.050	0.079	C45	0.311	0.575	0.279	574	6.36
C6	0.072	0.041	0.024	C45	0.311	0.575	0.279	600	7.20
C7	0.069	0.039	0.032	C45	0.311	0.575	0.279	590	6.95
C9	0.065	0.032	0.039	C45	0.311	0.575	0.279	578	6.59
C10	0.067	0.043	0.044	C45	0.311	0.575	0.279	584	6.77
C12	0.075	0.041	0.038	C45	0.311	0.575	0.279	608	7.29
Sl-22‡ (*retrograde stage*)									
Cl	0.055	0.031	0.027	C42	0.306	0.567	0.283	548	5.31
C2	0.054	0.042	0.027	C42	0.306	0.567	0.283	545	5.32
C3	0.065	0.039	0.025	C42	0.306	0.567	0.283	581	6.05
C4	0.067	0.041	0.024	C42	0.306	0.567	0.283	587	6.20
C5	0.068	0.039	0.026	C42	0.306	0.567	0.283	590	6.23
C39	0.049	0.028	0.022	C38	0.323	0.570	0.280	514	4.97
K-5§ (*retrograde stage*)									
D4	0.072	0.053	0.091	D14	0.341	0.573	0.282	571	6.00
D5	0.075	0.037	0.057	D14	0.341	0.573	0.282	580	6.33
D6	0.072	0.030	0.055	D14	0.341	0.573	0.282	572	6.12
D7	0.068	0.023	0.048	D14	0.341	0.573	0.282	560	5.88
D8	0.059	0.017	0.050	D14	0.341	0.573	0.282	533	5.27
D9	0.056	0.024	0.044	D14	0.341	0.573	0.282	524	5.16

**Grt*: $X_{Mg} = Mg/(Mg + Fe)$, $X_{Ca} = Ca/(Ca + (Mg + Fe))$, $X_{Mn} = Mn/(Mn + Ca + (Mg + Fe))$; *Bt*: $X_{Mg} = Mg/(Mg + Fe)$, $X_{Al} = Al/2/(Mg + Fe + Al/2)$, $X_{Si} = Si/(Mg + Fe + Si)$.

†*PT*-parameters for prograde stage are calculated using typical composition of Bt_1 in SL-22 (C45) and analyzed *Ms* composition ($X_{Na} = 0.11, X_{Al}^{M2} = 0.81$).

‡*PT*-parameters for retrograde stage are calculated using typical compositions of Bt_2 in SL-22 (C42, C38) and analyzed *Ms* composition (C32: $X_{Na} = 0.11, X_{Al}^{M2} = 0.81$).

§*PT*-parameters for retrograde stage are calculated using typical composition of Bt_2 in K-5 (D14) with analyzed *Ms* composition (D16: $X_{Na} = 0.08, X_{Al}^{M2} = 0.82$)

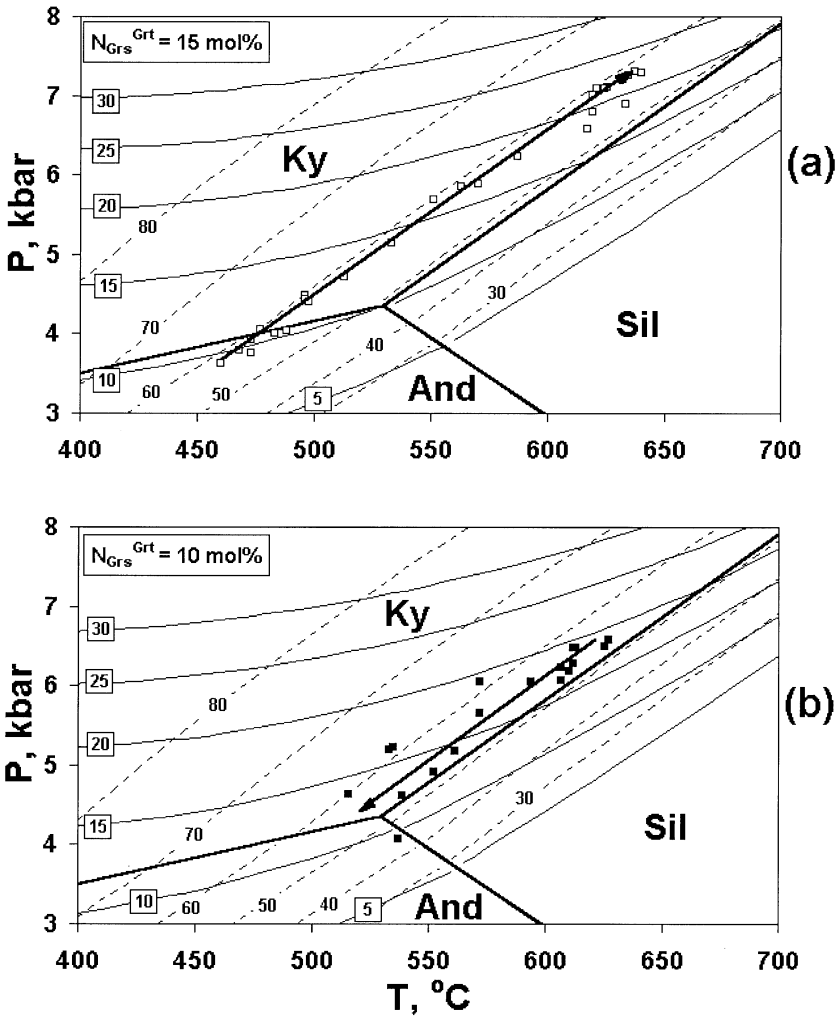

Fig. 7. *P-T* paths illustrating the prograde (**a**) and retrograde (**b**) stages of the evolution of sheared rocks from the TB recorded in the assemblage $Grt + Bt + Qtz + Ms + St + Mag + Pl \pm Chl \pm Ky$ of three samples from the chlorite-staurolite and kyanite-biotite metamorphic zones (Table 2). Temperature calculated with the biotite-garnet thermometer (*Perchuk*, 1989, 1990) and pressure determined by the modified *Grt-Ms-Bt-*Al_2SiO_5*-Qtz* barometer (Equation A2 in Appendix 2). N_{Mg} isopleths for garnet (solid lines) and biotite (dashed lines) calculated at a given N_{Ca}^{Grt} (left upper side). Arrows show direction of *P-T* paths

toward the surface, corresponding to the profiles of the garnet end members in Fig. 4 (Lap-15). As seen from Fig. 7b, the mineral associations preserved in the rocks under consideration do not record the end of the cooling history during their ascent towards the Earth's surface as late andalusite has not been found in the rocks.

Hout River Shear Zone

The equilibrium temperatures for the HRSZ were calculated using the *Bt-Grt* thermometer (*Perchuk*, 1990; *Perchuk* et al., 1996). For estimates of pressures the semi-empirical geobarometer (*Perchuk* et al., 1996; *Gerya* et al., 1997) was used based on the reaction:

$$Prp + 2Ms + Phl = 6Qtz + 3East \quad (3)$$

This reaction shows large volume changes and does not depend on water activity. However reaction (3) greatly depends on *P-T* parameters and activity coefficients for garnet and mica solid solutions. Recent publication of a new thermodynamic

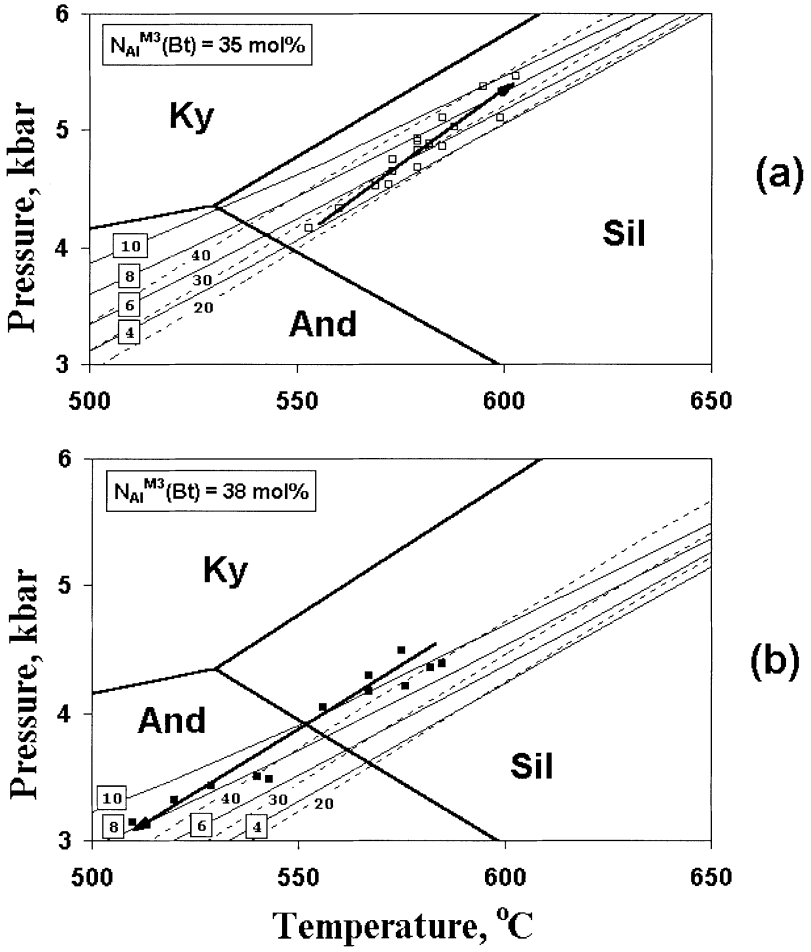

Fig. 8. *P-T* paths illustrating the prograde (**a**) and retrograde (**b**) stages of the evolution of sheared rocks from the HRSZ recorded in the assemblage $Grt + Bt + Qtz + Ms + Pl$ of two samples of mica schists (Table 2). Temperature calculated with the biotite-garnet thermometer (*Perchuk*, 1989, 1990) and pressure determined by the *Grt-Ms-Bt-Qtz* barometer (Equation A9 in Appendix 2). N_{Mg} isopleths for garnet (solid lines) and biotite (dashed lines) calculated at a given N_{Al}^{M3} in *Bt* (left upper side). Arrows show direction of *P-T* paths

data set (*Holland* and *Powell*, 1998) allows for the correction of previous formulation of the Gibbs free energy of reaction (3) (see Appendix 2).

Figure 8 shows the evolution of *P-T* parameters for the garnet-biotite-muscovite-quartz schists SL22 and K5 (see Table 1) at prograde (Fig. 8a) and retrograde (Fig. 8b) stages of metamorphism. These samples preserved the high-temperature portion of the prograde *P-T* path that also reflects heating and burial of the rocks to a crustal level of about 17 km ($P = 5.5$ kbar) at a temperature of about 610 °C. The retrograde stage is even better preserved in mineral assemblages recording their exhumation to a crustal level of about 10 km ($P = 3.3$ kbar) at $T = 520$ °C.

A model for the *P-T* evolution of the mica schists as a result of the emplacement of the granulites

Tanaelv Belt

Both detailed structural and geothermobarometric studies of the continuous prograde (Dl) and retrograde (D2) deformational history of sheared rocks from the TB showed that the rocks were subducted underneath the Lapland HGT and subsequently uplifted together with the granulites (*Perchuk* and *Krotov*, 1998). Evidence for a second plastic deformational event (D2), that is widely preserved in mica schists, is apparent in folding, microfolding, and tectonic melange developed in rocks of different rheological properties.

These deformations correspond to the formation of D2 folds in migmatites from the Lapland granulite complex. No rotated garnet porphyroblasts were formed at this stage. The euhedral porphyroblasts of many Fe-Mg minerals grew during and after the D2 deformation. Peak metamorphism occurred at 600–700 °C , at depths of about 20 km, i.e. in the mid-Precambrian crust (Fig. 9). The intensity of deformation suggests that the rocks lost their rigidity resulting in a decrease in viscosity which allowed the schists to flow. A similar scenario was obtained through numerical modeling of the geodynamics of metamorphic processes (*Perchuk* et al., 1992). In other words, equilibrium hydrostatic pressure always suggests deep plastic deformation.

Figure 9a provides a generalized insight into the *P-T* evolution of, not only the TB schists, but also of the juxtaposed granulites of the Lapland complex. The thermal peak of metamorphism of the mica schist coincides with the minimum *P-T* estimates for the cooling and ascent of the Lapland granulites along its southern border. This suggests that the granulites were exhumed simultaneously with the TB sheared rocks (*Perchuk* and *Krotov*, 1998). This suggestion is supported by a closing temperature (568 °C) and pressure (4.3 kbar) calculated for metapelites from the Northern Marginal Zone of the Lapland granulite complex (*Perchuk* et al., 2000).

Hout River Shear Zone

Figure 9b shows prograde and retrograde *P-T* paths for the garnet-bearing mica schists described above. These paths form a *P-T* loop reflecting the heating and

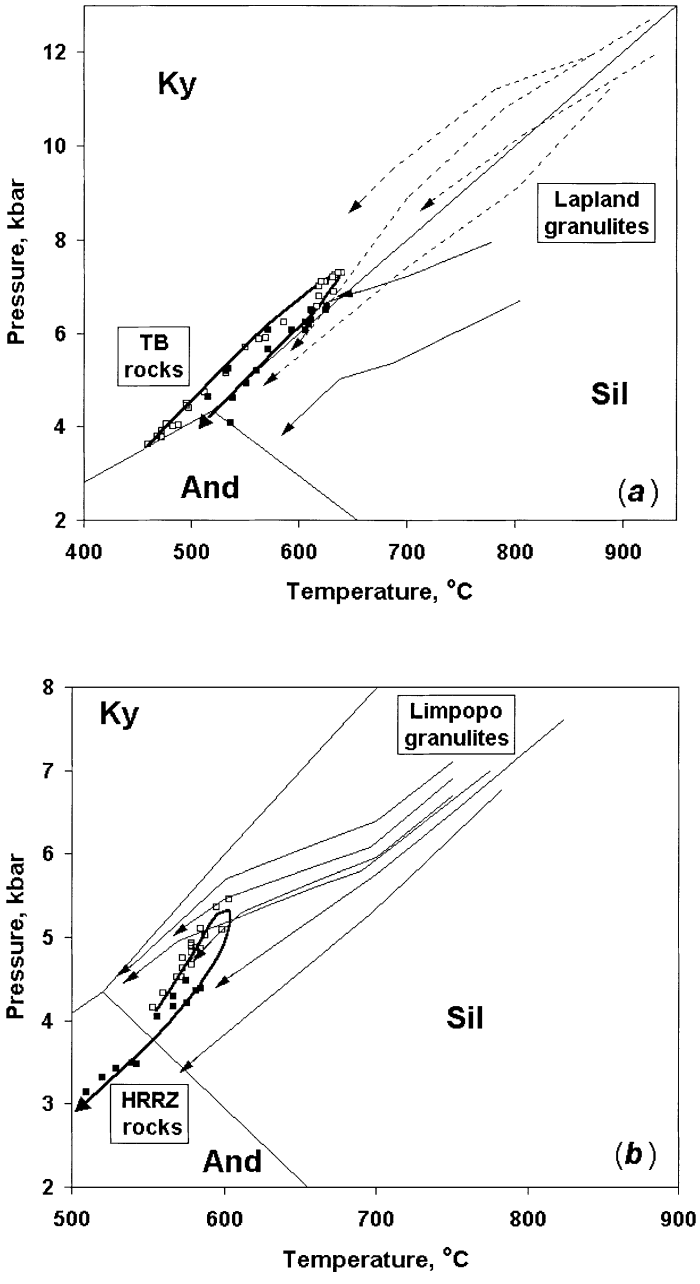

Fig. 9. Joint *P-T* evolution of the Lapland (**a**) and Limpopo (**b**) granulite complexes and sheared rocks of the TB and the HRSZ of the adjacent cratons. *P-T* paths for the granulites: dashed lines after *Fonarev* et al. (1994) and solid lines after *Perchuk* et al. (2000)

burial of rocks from a depth of about 12 km and $T = 550\,^{\circ}C$ to a depth of about 17 km at a temperature of $\sim 600\,^{\circ}C$. At this depth the temperature gradient that existed between the cooling Limpopo granulites and underthrusted KVG rocks (amphibolites with thin layers of mica schists) decreased. The subsequent thermal

and dynamic evolution of these units were similar with both having been exhumed to upper crustal levels of the Earth (Fig. 9b).

Published collisional models (e.g., *Thompson*, 1990) do not explain the burial of cratonic rocks to depths of about 20–25 km, and their subsequent ascent to the surface (as is suggested by preserved systematic chemical zoning of Fe-Mg minerals from the TB and HRSZ). In this context an alternative model is suggested by gravitation redistribution of rocks within the Precambrian Earth's crust (*Ramberg*, 1981; *Perchuk*, 1989, 1991) caused by mantle-derived fluid-heat flow. The observed circulation (Fig. 9) of metapelitic rocks preserved within the TB and the HRSZ therefore could have resulted from the ascent of the Lapland and Limpopo complexes through a mechanism of gravitation redistribution.

The mechanism of gravitation redistribution was first proposed (*Perchuk* et al., 1996) in order to explain the non-isobaric metamorphic zoning discovered within some of the sheared greenstones (2689 ± 7 Ma, *Kreissig* and *Holzer*, 1997) of the HRSZ (2671 ± 7 Ma, *Kreissig* and *Holzer*, 1997). The Limpopo granulite complex overlies rocks of the KVC and shows an intrusive-like, harpolith morphology (see Fig. 3 in *Perchuk* et al., 1999). As follows from the theory of gravitation redistribution (*Ramberg*, 1981; *Perchuk*, 1991; *Perchuk* et al., 1992), the ascent of granulites from the Earth's lower crust generates an opposite movement of the adjacent cratonic rocks. In this case, denser and cooler greenstones, which often compose the upper parts of Archean sequences, descended to depths of about 20 km and then returned toward the surface as a result of convection flow experiencing metamorphism under conditions of lower amphibolite facies. If this is the case, the staurolite schists in contact with the Limpopo granulite body must be similar in age to the adjacent granulites as was the case with the TB. The U-Pb data by *Kreissig* and *Holzer* (1997) on zircons from kyanite schists and adjacent granulites supports this suggestion.

Conclusions

Sheared rocks, such as the mica schists of the TB and the HRSZ separate the granulites of the Lapland and Limpopo HGT from the adjacent cratons. These lithologies, typical of the unsheared rocks of the greenstone belts, were underthrusted as a result of the emplacement of the granulite complex. A comparative petrology of the rocks from the TB and the HRSZ clearly indicates systematic similarities in their formation and evolution; this is recorded in rock structures, mineral chemistry and the *P-T* evolution. The analysis of microtextures and the application of geothermobarometry demonstrated that these sheared rocks experienced prograde metamorphism during a relatively rapid descent to depths of about 20 km ($P = 5.5$–7 kbar and $T \sim 600\,^{\circ}$C). The same rocks then experienced retrograde metamorphism during their subsequent ascent to a depth of about 10–15 km. According to the model of gravitation redistribution (*Perchuk*, 1989, 1991; *Perchuk* et al., 1992) such a circulation could have been caused by a mechanism of crustal convection, which was promoted by the ascent of a large granulite body between two greenstone cratons, as was the case with both the Lapland and the Limpopo complexes.

Appendix 1: Abbreviations and symbols

Table A1-1. *Table of mineral symbols used*

Symbol	Mineral	Symbol	Mineral	Symbol	Mineral
Alm	almandine	*Ged*	gedrite	*Phl*	phlogopite
Ant	anthophyllite	*Grt*	garnet	*Pl*	plagioclase
Ap	apatite	*Grs*	grossular	*Prp*	pyrope
And	andalusite	*Ilm*	ilmenite	*Qtz*	quartz
Bt	biotite	*Kfs*	K-feldspar	*Sil*	sillimanite
Chl	chlorite	*Ky*	kyanite	*Sps*	spessartite
Ep	epidote	*Mag*	magnetite	*St*	staurolite
East	eastonite	*Ms*	muscovite	*Tur*	turmaline

Table A1-2. *Abbreviations for major geological units*

Abbreviations	Full name	Isotopic age, Ga
HGT	High grade terrain	Lapland: 1.9–1.85 Limpopo: $\sim$ 2.65
KC	Karelian craton	3.1–2.7
IC	Inari Craton	>2.8
KVC	Kaapvaal Craton	>2.7
ZC	Zimbabwe craton	>2.7
HRSZ	Hout River Shear Zone (Limpopo area)	2.65
BC	Belomorian Complex of the Karelian craton	>2.8
SMZ	Southern Marginal Zone of the Limpopo HGT	2.63
TB	Tanaelv (Tana) Belt of the Lapland area	2.46–1.9
KTG	Korva Tundra Group of the TB	1.9
KG	Kandalaksha group of the TB	2.46–1.9
KB	Kola Central Block	2.9–2.65
PC	Pechenga Complex	2.46–1.85
MB	Murmansk Block	2.9–2.45

Appendix 2: The evaluation of semi-empirical internally consistent geothermobarometers

Thermodynamic symbols used

X_i = mole fraction of component i in a phase, for example $X_{Mg} = Mg/(Mg + Fe)$; N_i = mole per cent of component i in a phase; $X^{fl}_{CO_2}$ = mole fraction of CO_2 in a fluid (fl); $X^{fl}_{H_2O}$ = mole fraction of H_2O in a fluid; γ_i = activity coefficient of component i in a phase; $a_i = \gamma_i\ X_i$ = activity of component i in a mineral; T = temperature; P = pressure in kbar; G = Gibbs free energy change of reaction r, cal/mole; $R = 1.987$ cal/mole K; $G^e_i = RT \ln\gamma_i$ = excess partial molar energy, cal/mole.

Reaction

$$1/3Phl + 2/3Al_2SiO_5 + 1/3Qtz = 1/3Prp + 1/3Ms \qquad \text{(A1)}$$

In general form the change in Gibbs free energy for this reaction should be written as following:

$$\Delta G(\mathrm{A1}) = 1.987T \ln[X_{Prp}^{Gr}/X_{\mathrm{Mg}}^{Bt}] + \Delta H(\mathrm{A1}) - T\Delta S(\mathrm{A1}) + P\Delta V(\mathrm{A1}) + G_{Prp}^{eGrt} = 0 \quad (\mathrm{A2})$$

However the ΔG(A1) value is strongly controlled by properties of a particular Al_2SiO_5 polymorph variety. In this paper we have used the latest version of the thermodynamic data set of *Holland* and *Powell* (1998) that gives the following changes in ΔH(A1), ΔS(A1), and ΔV(A1):

Al_2SiO_5	ΔH(A1)	ΔS(A1)	ΔV(A1)
Sil	789.9	− 3.744	− 0.373
And	1852.8	− 2.55	− 0.393
Ky	1959	− 1.78	− 0.279

and $X_{\mathrm{Mg}}^{Bt} = \mathrm{Mg}/(\mathrm{Fe} + \mathrm{Mg}), X_{Prp}^{Grt} = \mathrm{Mg}/(\mathrm{Fe} + \mathrm{Mn} + \mathrm{Mg} + \mathrm{Ca})$. The expression for the excess partial molar Gibbs free energy, G_{Prp}^{eGrt}, for the pyrope end-member in garnet as a function of temperature

$$G_{Prp}^{eGrt} = RT \ln[\gamma_{Prp}^{Grt}] = X_{\mathrm{Ca}}^{Grt}[X_{\mathrm{Ca}}^{Grt}(3300 - 1.5T) + X_{\mathrm{Fe}}^{Grt}(5704 - 1.24T)] \quad (\mathrm{A3})$$

was taken from the paper by *Aranovich* and *Podlesskii* (1989), where $X_{\mathrm{Fe}} = \mathrm{Fe}/(\mathrm{Fe} + \mathrm{Mg} + \mathrm{Ca} + \mathrm{Mn})$ and $X_{\mathrm{Ca}} = \mathrm{Ca}/(\mathrm{Fe} + \mathrm{Mg} + \mathrm{Ca} + \mathrm{Mn})$.

Reaction

$$Prp + 2Ms + Phl = 6Qtz + 3East \quad (\mathrm{A4})$$

The standard Gibbs free energy change for reaction (3) calculated at $0.5 < P < 10$ kbar and $400 < T < 800\,^{\circ}\mathrm{C}$ was approximated by the equation

$$\Delta G^{0}(\mathrm{A4})(+/- 69\ \mathrm{cal}) = -11043.4 + 5.2841T + 0.86356P, \quad (\mathrm{A5})$$

This equation can be used for assemblages of both the TB and the HRSZ. In this form, however, this equation is not internally consistent with eq. (A2). The compositions of coexisting *Grt*, *Bt*, and *Ms* from the TB mica schists were used in order to achieve internal consistency of the *Grt-Bt-Ms-Ky-Qtz* and *Grt-Bt-Ms-Qtz* geobarometers. As a result the $\Delta H^{\circ}(\mathrm{A4}) = -11043.4$ cal of eq. (A5) was changed to −9420 cal at the following activities of *Phl* and *East* in the biotite solid solution

$$RT \ln a_{Phl} = RT \ln(X_{\mathrm{K}}^{\mathrm{A}} \cdot X_{\mathrm{Mg}}^{\mathrm{M1}} \cdot X_{\mathrm{Mg}}^{\mathrm{M2}} \cdot X_{\mathrm{Mg}}^{\mathrm{M3}} \cdot X_{\mathrm{Al}}^{\mathrm{T1}} \cdot X_{\mathrm{Si}}^{\mathrm{T1}}) + 2390[(X_{\mathrm{Al}}^{\mathrm{M3}})^2 + X_{\mathrm{Al}}^{\mathrm{M3}} \cdot X_{\mathrm{Fe}}^{\mathrm{M3}}], \quad (\mathrm{A6})$$

$$RT \ln a_{East} = RT \ln(X_{\mathrm{K}}^{\mathrm{A}} \cdot X_{\mathrm{Mg}}^{\mathrm{M1}} \cdot X_{\mathrm{Mg}}^{\mathrm{M2}} \cdot X_{\mathrm{Al}}^{\mathrm{M3}} \cdot (X_{\mathrm{Al}}^{\mathrm{T1}})^2] + 2390[(X_{\mathrm{Mg}}^{\mathrm{M3}})^2 + X_{\mathrm{Mg}}^{\mathrm{M3}} \cdot X_{\mathrm{Fe}}^{\mathrm{M3}}], \quad (\mathrm{A7})$$

where $X_K^A = K/(K + \mathrm{Na}), X_{\mathrm{Mg}}^{\mathrm{M1}} = X_{\mathrm{Mg}}^{\mathrm{M2}} = \mathrm{Mg}/(\mathrm{Mg} + \mathrm{Fe}), X_{\mathrm{Al}}^{\mathrm{M3}} = [7\mathrm{Al}/(\mathrm{Al} + \mathrm{Mg} + \mathrm{Fe} + \mathrm{Si} + \mathrm{Ti}) - 1]/2, X_{\mathrm{Mg}}^{\mathrm{M3}} = X_{\mathrm{Mg}}^{\mathrm{M1}}(1 - X_{\mathrm{Al}}^{\mathrm{M3}}), X_{\mathrm{Fe}}^{\mathrm{M3}} = 1 - X_{\mathrm{Al}}^{\mathrm{M3}} - X_{\mathrm{Mg}}^{\mathrm{M3}}, X_{\mathrm{Al}}^{\mathrm{T1}} = (1 + X_{\mathrm{Al}}^{\mathrm{M3}})/2, X_{\mathrm{Si}}^{\mathrm{T1}} = 1 - X_{\mathrm{Al}}^{\mathrm{T1}}$.

Equations (A6) and (A7) were derived using a multi-sites *Phl-East* solid solution model (*Holland* and *Powell*, 1998) and an ideal Fe-Mg mixing model of biotite (*Perchuk*, 1990). The latter is based on the experimental data by *Perchuk* and *Lavrent'eva* (1983) for the Grt-Bt exchange equilibrium studied for a wide Fe-Mg range of compositions. The mixing property of the muscovite-paragonite solid solution were calculated using a multi-sites model (*Holland* and *Powell*, 1998) and experimental data of *Eugster* et al. (1972). Thus, the Gibbs partial molar mixing free energy for muscovite can be calculated with the following equation

$$RT\ln a_{Ms} = RT\ln(4X_{\mathrm{K}}^{\mathrm{A}}\cdot X_{\mathrm{Al}}^{\mathrm{M2}}\cdot X_{\mathrm{Al}}^{\mathrm{T1}}\cdot X_{\mathrm{Si}}^{\mathrm{T1}}) + (4164 + 0.395T + 0.126P)[2(X_{\mathrm{Na}}^{\mathrm{A}})^3 - (X_{\mathrm{Na}}^{\mathrm{A}})^2] + (3082 + 0.170T + 0.082P)[2(X_{\mathrm{Na}}^{\mathrm{A}})^2 - 2(X_{\mathrm{Na}}^{\mathrm{A}})^3] \quad \text{(A8)}$$

where $X_{\mathrm{K}}^{\mathrm{A}} = \mathrm{K}/(\mathrm{K}+\mathrm{Na}), X_{\mathrm{Na}}^{\mathrm{A}} = 1 - X_{\mathrm{K}}^{\mathrm{A}}, X_{\mathrm{Al}}^{\mathrm{M2}} = 1 - 6(\mathrm{Mg}+\mathrm{Fe})/(\mathrm{Al}+\mathrm{Mg}+\mathrm{Fe}+\mathrm{Si}), X_{\mathrm{Al}}^{\mathrm{T1}} = 0.5X_{\mathrm{Al}}^{\mathrm{M2}}, X_{\mathrm{Si}}^{\mathrm{T1}} = 1 - X_{\mathrm{Al}}^{\mathrm{T1}}$. For calculating the *Prp* activity in the *Alm-Sps-Grs-Prp* garnet solid solution we used equation (A3). Thus, the pressure calculations using compositions of *Grt*, *Bt*, and *Ms* from mica schists can be done with the formula

$$P\ \mathrm{bar} = (9420 - 5.2841T - G^e)/(0.86356 - 2V^{eMs}) \quad \text{(A9)}$$

where

$$G^e = 3RT\ln a_{East} - RT\ln a_{Prp} - RT\ln a_{Phl} - 2(RT\ln a_{Ms} - V^{eMs}P) \text{ and } V^{eMs} = 0.126[2(X_{\mathrm{Na}}^{\mathrm{A}})^3 - (X_{\mathrm{Na}}^{\mathrm{A}})^2] + 0.082[2(X_{\mathrm{Na}}^{\mathrm{A}})^2 - 2(X_{\mathrm{Na}}^{\mathrm{A}})^3].$$

Acknowledgments

Since 1995 this work was carried out as part of the RF-RSA collaboration supported by FRD, Gencor and JCI grants to *DDvR*, RFBR grants (# 96-05-64396, #96-15-98470 and #99-05-65602) to *LLP*. This paper benefited greatly through helpful reviews by *J. Barton*, *A. A. Grafchikov* and *A. V. Konilov*.

References

Aranovich LYa, Podlesskii KK (1989) Geothermobarometry of high-grade metapelites: simultaneously operating reactions. J Geol Soc Lond Spec Publ 1988: 41–65

Barbey P, Raith M (1990) The granulite belt of Lapland. In: *Vielzeuf D, Vidal Ph* (eds) Granulites and crustal evolution. Kluwer, Dordrecht, pp 111–132 (NATO Asi Series C)

Barbey P, Convert J, Martin M, Moreau B, Capdevila R, Hameurt J (1980) Relationships between granite-gneiss terrains, greenstone belts and granulite belts in the Archean crust of Lapland (Fennoscandia). Geol Rdsch 69: 648–658

Barbey P, Convert J, Moreau B, Capdevila R, Hameurt J (1984) Petrogenesis and evolution of an Early Proterozoic collisional orogen: the Granulite Belt of Lapland and the Belomorides (Fennoscandia). Bull Geol Soc Finl 56: 161–188

Barton JM (Jr), du Toit MC, Van Reenen DD, Ryan B (1983) Geochronological studies in the Southern Marginal Zone of the Limpopo mobile belt, southern Africa. Geol Soc S Afr Spec Publ 8: 55–64

Bernard-Griffits J, Peucat JJ, Postaire B, Vidal P, Convert J, Moreau B (1984) Isotopic data (U-Pb, Rb-Sr, Pb-Pb and Sm-Nd) on mafic granulites from Finnish Lapland. Precamb Res 23: 225–348

Bersthelsen A, Marker M (1986) Tectonics of the Kola collision suture and adjacent Arechean and Early Proterozoic terrains in the north-eastern region of the Baltic shield. Tectonophysics 126: 31–55

Bibikova EV, Melnikov VF, Avakyan KKh (1993) Lapland granulites: petrology, geochemistry and isotopic age. Petrology 1: 215–234

Carmichael DL (1970) Intersecting isograde in the Whetstone Lake Area, Ontario. J Petrol 11: 147–181

Daly J, Glebovitskii S (1991) Timing of the metamorphism in the Lapland granulite belt, Finland. Res Terrae (ser A) 5: 11

de Beer JH, Stettler EH (1992) The deep structure of the Limpopo belt from geophysical studies. Precamb Res 55: 173–186

de Wit MJ, Ashwal LD (1997) Greenstone belts. Clarendon Press, Oxford, 809 pp

de Wit MJ, Roering C, Hart RJ, Armstrong RA, De Conde CEJ, Green RWE, Tredoux M, Pederdy E, Hart RA (1992a) Formation of an Archean continent. Nature 357: 553–562

de Wit MJ, van Reenen DD, Roering C (1992b) Geologic observations across a tectono-metamorphic boundary in the Babangu area, Giyani (Sutherland) Greenstone Belt, South Africa. Precamb Res 55: 111–122

Eskola P (1952) On the granulites of Lapland. Am J Sci (*Bowen Volume*) 1:133–171

Eugster HP, Albee AL, Bence AE, Thompson JB, Waldbaum DR (1972) The two-phase region and excess mixing properties of paragonite-muscovite crystalline solution. J Petrol 13: 147–179

Fonarev VI, Grafchikov AA, Konilov AN (1994) Experimental investigations of equilibria involving mineral solid solutions. In: *Zharikov VA, Fedkin VV* (eds) Experimental problems in geology. Nauka Press, Moscow, pp 323–355 (in Russian)

Gaal G, Berthelsten A, Gorbatchev R (1989) Structure and composition of the Precambrian crust along the POLAR profile in the northern Baltic Shield. Tectonophysics 162: 1–25

Gerya TV, Perchuk LL, Triboulet C, Audren C, Ses'ko AI (1997) Petrology of the Tumanshet metamorphic complex, eastern Sayan, Siberia. Petrology 5 (6): 503–533

Glebovitskii MN, Efimov MM (1997) Belomorian-Lapland early Precambrian high-grade mobilke belt EUG 9. Terra Nova [Abstracts Suppl I] 9: 363

Glebovitskii VA, Miller YuV, Drugova GM, Milkevich RI, Vrevskiy AB (1996) Structure and metamorphism of the Belomorian-Lapland collision Zone. Geotectonica 1: 63–75

Hiroi Y (1983) Progressive metamorphism of the Unazuki pelitic schists in the Hida Terrane, Central Japan. Contrib Mineral Petrol 82: 334–350

Holland TJB, Powell R (1998) Internally consistent thermodynamic data set for phases of petrological interest. J Metam Geol 16: 309–344

Holzer L, Frei R, Barton JM Jr, Kramers JD (1998) Unraveling the record of successive high grade events in the Central Zone of the Limpopo Belt using Pb single phase dating of metamorphic minerals. Precamb Res 87: 87–115

Hörmann PK, Raith M, Raase P, Ackermand D, Seifert F (1980) The granulite complex of Finnish Lapland: petrology and metamorphic conditions in the Ivalojoki-Inarijarvi area. Geol Surv Finl Bull 308: 1–95

Johnson SE (1993a) Unavailing the spirals: a serial thin-section study and three-dimensional computer-aided reconstruction of spiral-shaped inclusion trails in garnet porphyroblasts. J Metam Geol 11: 621–634

Johnson SE (1993b) Testing models for the development of spiral-shaped inclusions trails in garnet porphyroblasts: to rotate not to rotate, that is the question. J Metam Geol 11: 635–659

Johnson SE, Bell TH (1996) How useful are millipede' and other similar porphyroblast microstructures for determining synmetamorphic deformation histories? J Metam Geol 14: 15–28

Kozlov NE, Ivanov AA, Nerovich LI (1990) The Lapland granulite belt (primary origin and evolution). RAS Press, Kola Scientific Centre, Apatity, 231 pp (in Russian)

Krill AG (1985) Svecokarelian thrusting with thermal inversion in the Karasjok-Levajok area of the northern Baltic Shield. Nor Geol Unders 403: 89–101

Kreissig K, Holzer L (1997) The Kaapvaal craton–Southern Marginal Zone (Limpopo belt) connection; implications from geochronological data, Pb isotopes and REE patterns. Terra abstracts (EUG 9). Terra Nova [Abstracts Suppl I] 9: 364–365

Laird J (1991) Chlorites: metamorphic petrology. In: *Bailey SW* (ed) Hydrous phyllosilicates (exclusive micas). Rev Mineral 19: 415–454

Latyshev LN (1967) Geological structure of the Korva Tundra Formation in southern framing of the Lapland granulite complex. In: Problems of geology, mineralogy and geochemistry of volkanic and metamorphic complexes. USSR Acad Sci Kola Brench, Apatity, pp 55–57 (in Russian)

Latyshev LN (1971) Stratigraphy of supracrustal rocks of the Korva Tundra. In: Stratigraphic division and correlation of the Precambrian in the northeastern part of the Baltic shied. Apatity, pp 61–65 (in Russian)

Lobach-Zhuchenko SB, Bibikova EV, Drugova GM, Beliackiy EV, Gracheva TV, Amelin YuV, Matrenichev VA (1993) Geochronology and petrology of magmatic complex of the Tupaya Guba, N-W Belomorie, Kola Peninsula. Petrology 1(6): 657–677

Marker M (1988) Early Proterozoic thrusting of the Lapland granulite belt and its geotectonic evolution, northern Baltic Shield. Geol Foren Stockh Forh 110: 405–410

Marker M (1990) Tectonic interpretation and new crustal modeling along the POLAR Profile, Northern Baltic Shield. In: *Freeman R, Mueller S* (eds) Data compilations and synoptic interpretation. 6th Workshop on the European geotraverse project. Proc Eur Sci Found, Strasbourg, pp 9–22

Marker M (1991) Metamorphism, deformations and structure of the crust. In: *Tuisku P, Laajoki K* (eds) Excursion guide to Lapland. University of Oulu, Finland, pp 38–66

McCourt S, van Reenen DD (1992) Structural geology and tectonic setting of the Sutherland Greenstone Belt, Kaapvaal Craton, South Africa. Precamb Res 55: 93–110

McCourt S, Vearncombe JR (1992) Shear zones of the Limpopo Belt and adjacent granitoid-greenstone terranes: Implications for late Archean collision tectonics in southern Africa. Precamb Res 55: 553–570

Merilainen K (1976) The granulite complex and adjacent rocks in Lapland, Northern Finland. Geol Surv Finl Bull 281: 1–129

Miyashiro A (1973) Metamorphism and metamorphic belts. Allen and Unwin, London, 386 pp

Mikkola E (1937) Pre-Quaternary rocks, sheets C7 and D7, Sodankyta, Tuntajoki. General Geological Map of Finland 1:400 000. Geol Toimikunta, Helsinki

Mikkola E (1941) General geological map of Finland. Sheets B7, C7, D7, Muonio, Sodankyta, Tuntajoki. Explanation to the map of rocks, Suomen. Geol Toimikunta Helsinki, 286 pp

Mints MV, Glaznev VN, Konilov AN (1996) The Early Precambrian of the north-eastern Baltic shield: paleogeodynamics, crustal structure, and evolution. Science World Press, Moscow, 312 pp (in Russian, with extended English Abstract)

Mitrofanov FP, Balagansiy VV, Balashov Yu A (1993) U-Pb age of gabbroanorthosites from the Kola Peninsula. Dokl Rus Akad Nauk 331(1): 95–98

Miyano T, Ogata H, van Reenen DD, Van Schalkwyk JF, Arakawa Y (1990) Peak metamorphic conditions of sapphirine- bearing rocks in the Rhenosterkoppies Greenstone

Belt, northern Kaapvaal Craton, South Africa. In: *Glover JC, Ho SE* (eds) The Archean: Terranes. Processes and Metallogeny 22: 73–87

Perchuk LL (1973) Thermodynamic regimes of deep-seated petrogenesis. Nauka Press, Moscow, 301 pp (in Russian)

Perchuk LL (1977) Thermodynamic control of metamorphic processes. In: *Saxena SK, Bhattacharji S* (eds) Energetics of geological processes. Springer, New York, pp 285–352

Perchuk LL (1989) P-T-fluid regimes of metamorphism and related magmatism with specific reference to the Baikal Lake granulites. In: *Daly S, Yardley DWD, Cliff BO* (eds) Evolution of metamorphic belts. Geol Soc Lond Spec Publ 42: 275–291

Perchuk LL (1990) Derivation of thermodynamically consistent system of geothermometers and geobarometers for metamorphic rocks and magmatic. In: *Perchuk LL* (ed) Progress in metamorphic and magmatic petrology. Cambridge University Press, Cambridge, pp 93–112

Perchuk LL (1991) Studies in magmatism, metamorphism, and geodynamics. Intern Geol Rev 33: 311–374

Perchuk LL, Lavrent'eva IV (1983) Experimental investigation of exchange equilibria in the system cordierite-garnet-biotite. In: *Saxena SK* (ed) Kinetics and equilibrium in mineral reactions. Springer, New York, pp 199–240

Perchuk LL, Gerya TV (1995) Studies of the boundaries between granulite facies terrains and cratons. Centennial Geocongress, Extended Abstracts. Geol S South Afr 2: 622–623

Perchuk LL, Krotov AV (1998) Petrology of the mica schists of the Tanaelv belt in the southern tectonic framing of the Lapland granulite complex. Petrology 6(2): 149–179

Perchuk LL, Aranovich LYa, Podlesskii KK, Lavrent'eva IV, Gerasimov VYu, Fed'kin VV, Kitsul VN, Karsakov LP (1985) Precambrian granulites of the Aldan shield, eastern Siberia, USSR. J Metam Geol 3: 265–310

Perchuk LL, Podladchikov YuYu, Polaykov AN (1992) Geodynamic modeling of some metamorphic processes. J Metam Geol 10: 311–318

Perchuk LL, Gerya TV, van Reenen DD (1996) The Limpopo metamorphic complex, South Africa. 2. Decompression/cooling regimes of granulites and adjusted rocks of the Kaapvaal craton. Petrology 4(6): 571–599

Perchuk LL, Gerya TV, van Reenen DD, Smit CA (1997) Cratonization: from greenstone belts to granulite EUG 9. Terra Nova [Abstracts Suppl I] 9: 362

Perchuk LL, Gerya TV, van Reenen DD, Krotov AV, Safonov OG, Smit CA, Shur MYu (2000) Comparable petrology and metamorphic evolution of the Limpopo (South Africa) and Lapland (Fennoscandia) high-grade terrains. Mineral Petrol (this volume)

Pozhilenko VI, Smolkin VF, Sharov NV (1997) Seismic-geological models for the Earth's crust in the Lapaland-Pechenga region, Russia. In: *Sharov NV* (ed) A seismological model of the Lithosphere of Northern Europe: Lapland-Pechenga region. Kola Scientific Center, Russian Academy of Sciences, Apatity, pp 181–208 (in Russian)

Priyatkina LA, Sharkov EV (1979) Geology of the Lapland deep-seated fault. Nauka Press, Leningrad, 210 pp (in Russian)

Powell D (1966) On the preferred crystallographic orientation of garnet in some metamorphic rocks. Mineral Mag 35: 1094

Powell D (1970) Rotational fabrics in metamorphic minerals. Mineral Mag 37: 453–459

Powell D, Treagus JE (1967) On the geometry of S-shaped inclusion trails in garnet porphyroblasts. Mineral Mag 36: 453–456

Przhjialgovskiy E, Terekhov E (1995) Karasjok-Belomorian parautochton (2.2–1.9 Ga) and some aspects of structural and geochemical reworkig of rock complexes. Nor Geol Unders Spec Publ 7: 193–200

Raith M, Raase P, Hörmann PK (1982) The Precambrian of Finnish Lapland: evolution and regime of metamorphism. Geol Rdsch 71: 230–244

Ramberg H (1981) Gravity, deformation and geological application. Academic Press, New York, 418 p

Reinhard J, Rubenach MJ (1989) Temperature-time relationships across metamorphic zones: evidence from porphyroblast-matrix relationships in progressively deformed metapelites. Tectonophysics 158: 141–161

Roering C, van Reenen DD, Smit CA, Barton JM Jr, de Beer JH, de Wit MJ, Stettler EH, Van Schalkwyk JF, Stevens G, Pretorius S (1992a) Tectonic model for the evolution of the Limpopo Belt. Precamb Res 55: 539–552

Roering C, van Reenen DD, de Wit MJ, Smit CA, de Beer JH, Van Schalkwyk JF (1992b) Structural geological and metamorphic significance of the Kaapvaal Craton–Limpopo Belt contact. Precamb Res 55: 69–80

Rollinson HR, Blenkinsop TG (1995) The magmatic, metamorphic and tectonic evolution of the Northern Marginal Zone of the Limpopo Belt in Zimbabwe. J Geol Soc Lond 152: 65–75

Rosenfeld JL (1970) Rotated garnets in metamorphic rocks. Geol Soc Am (Spec Paper) 129: 1–49

Schoneveld C (1977) A study of some typical inclusion patterns in strongly paracrystalline-rotated garnets. Tectonophysics 39: 453–471

Smit CA, van Reenen DD (1997) Deep crustal shear zones, high-grade tectonics, and associated metasomatic alteration in the Limpopo belt, South Africa: implications for deep crustal processes. J Geol 29: 37–57

Smit CA, Roering C, van Reenen DD (1992) The structural framework of the southern margin of the Limpopo Belt, South Africa. Precamb Res 55: 51–67

Spy A (1963) Origin and significance of snowball structure in garnet. J Petrol: 211–222

Thompson AB (1990) Heat, fluids, and melting in the granulite facies. In: *Vielzeuf D, Vidal Ph* (eds) Granulites and crustal evolution. Kluwer, Dordrecht, pp 37–58 (NATO Asi Series C)

Treloar PJ, Coward MP, Harris NBW (1992) Himalayan-Tibetan analogies from the evolution of the Zimbabwe Craton and the Limpopo Belt, South Africa. Precamb Res 55: 571–587

Tsunogae T, Miyano T, Ridley J (1992) Metamorphic P-T profiles from the Zimbabwe Craton to the Limpopo Belt, Zimbabwe. Precamb Res 55: 259–277

Tuisku P, Laajoki K (1991) Metamorphism, deformation and structure of the crust. Excursion Guide to Lapland. Oulu (Finland) OUP: 76 p

van Reenen DD, Smit CA (1996) The Limpopo metamorphic complex, South Africa. 1. Geological setting and relationships between the granulite complex and the Kaapvaal and Zimbabwe cratons. Petrology 4(6): 562–570

van Reenen DD, Roering C, Brandl G, Smit CA, Barton JM (Jr) (1990) The granulite facies rocks of the Limpopo belt, southern Africa. In: *Vielzeuf D, Vidal Ph* (eds) Granulites and crustal evolution. Kluwer, Dordrecht, pp 257–289 (NATO Asi Series C)

van Reenen DD, Roering C, Ashwal LD, de Wit MJ (1992) The Archean Limpopo granulite belt: tectonics and deep crustal processes. Precamb Res 55(1–4): 587 p

van Schalkwyk JF, van Reenen DD (1992) High-temperature hydration of ultramafic granulites from the Southern Marginal Zone of the Limpopo Belt by infiltration of CO_2-rich fluid. Precamb Res 55: 337–352

van Schalkwyk JF, van Reenen DD, Barton JM (Jr) (1987) Greenschists to granulite metamorphism of ultramafic rocks in the northern Kaapvaal craton, southern Africa. Abst Geol Assoc Canada 12: 98

Volodichev OI (1990) Belomorian complex of Karelia (geology and petrology. Nauka Press, Leningrad, 215 pp (in Russian)

Authors' addresses: Prof. *L. L. Perchuk* and *A. V. Krotor*, Department of Petrology, Geological Faculty, Moscow State University, Vorbievy gory, Moscow, 119899 Russia, e-mail: llp@geol.msu.ru; *T. V. Gerya*, Institute of Experimental Mineralogy, Russian Academy of Sciences, Chernogolovka, Moscow district, 142432, Russia, e-mail: taras@iem. ac. ru; *D. D. Van Reenen* and *C. A. Smit*, Department of Geology, Rand Afrikaans University, Aukland Park, Johannesburg, P.O. Box 524, Republic of South Africa, 2006, e-mail: ddrv@na.rau.ac.za